TAMPEREEN TEKNILLINEN YLIOPISTO
TAMPERE UNIVERSITY OF TECHNOLOGY
Julkaisu 732 • Publication 732

Marja Niemi

Photoinduced Electron Transfer in Dyads and Triads of Porphyrins, Phthalocyanines and Fullerenes

Tampere 2008

Tampereen teknillinen yliopisto. Julkaisu 732
Tampere University of Technology. Publication 732

Marja Niemi

Photoinduced Electron Transfer in Dyads and Triads of Porphyrins, Phthalocyanines and Fullerenes

Thesis for the degree of Doctor of Technology to be presented with due permission for public examination and criticism in Festia Building, Auditorium Pieni Sali 1, at Tampere University of Technology, on the 30th of May 2008, at 12 noon.

Tampereen teknillinen yliopisto - Tampere University of Technology
Tampere 2008

ISBN 978-952-15-1963-5 (printed)
ISBN 978-952-15-1982-6 (PDF)
ISSN 1459-2045

Abstract

Photoinduced electron transfer of several dyads and triads consisting of porphyrins or phthalocyanines as electron donors and fullerene as acceptor was studied. Efficient electron transfer was observed in the studied compounds due to two important approaches in the design of the molecular structure: (i) appropriate selection of the donor and acceptor moieties and (ii) controlled orientation and distance of the moieties achieved with two covalent linkers connecting the donor and acceptor.

Mainly spectroscopic methods were used to determine the reaction schemes of the photoinduced reactions. Time-resolved spectroscopy revealed the transient states of electron transfer and it was confirmed that the intermediate exciplex state precedes the charge-separated state in all the studied compounds. Rate constants of the transitions and energies of the states were evaluated in both polar and non-polar solvents.

To test the possibility to use the studied compounds in solid state photovoltaic devices, thin films with porphyrin-porphyrin-fullerene triad structures were attached on glass substrates covered with a transparent indium tin oxide layer. The triad structures were obtained by building successive self-assembled monolayers (SAM) of porphyrin and porphyrin-fullerene dyad on top of each other. Because of the presence of the secondary electron donor, the triad structures were found to enhance both photocurrent and photovoltage generation compared to the corresponding porphyrin-fullerene dyad SAM.

Preface

First of all I want to thank my supervisor, Prof. Helge Lemmetyinen for giving me the opportunity to work in his excellent group and for believing that I could finish a Thesis related to physical chemistry even though my background was in neither physics nor chemistry. Prof. Nikolai Tkachenko, my second supervisor, deserves my deepest gratitude for all his help both in the theoretical and practical issues. In addition to his extensive knowledge, Kolja has incredible patience to explain things over and over again, which was indispensable for me and for this Thesis.

I wish to thank Dr. Alexander Efimov for the compounds, especially for all the hard work on the phthalocyanine dyads, and for his advice on the real chemistry. My warmest thanks go also to all the other co-authors of the papers, both at our own department and in Prof. Fukuzumi's and Prof. Imahori's groups in Osaka and Kyoto. Dr. Vladimir Chukharev I want to thank for all the practical help in the lab.

For the pleasant work atmosphere I am grateful to all the staff at the department. Special thanks go to Anne Kotiaho for being the best roommate one could hope for.

I want to thank my parents, Seija and Sakari, and brothers, Matti and Pekka, for supporting me in all the decisions I have made and especially my father for sharing my interest in science. My friends, Riina, Viitsu, Mari, Maija, Suvi and Mirja, I want to thank for their support and for all the fun. Last, but certainly not the least, I thank my husband, Eetu, and son, Lasse, for being everything to me. Without you this Thesis would not have been finished.

This work was carried out at the Department of Chemistry and Bioengineering, Tampere University of Technology between February 2004 and February 2008. The Graduate School of Tampere University of Technology is gratefully acknowledged for funding.

Tampere, February 2008

Marja Niemi

List of publications

The Thesis is based on the work contained in the following papers, which will hereafter be referred to by their Roman numerals:

I **Photoinduced Electron Transfer in Double-Bridged Porphyrin-Fullerene Triads**
Marja Isosomppi, Nikolai V. Tkachenko, Alexander Efimov and Helge Lemmetyinen
J. Phys. Chem. A **2005**, *109*, 4881-4890.

II **Photoinduced electron transfer in multilayer self-assembled structures of porphyrins and porphyrin-fullerene dyads on ITO**
Marja Isosomppi, Nikolai V. Tkachenko, Alexander Efimov, Kimmo Kaunisto, Kohei Hosomizu, Hiroshi Imahori and Helge Lemmetyinen
J. Mater. Chem. **2005**, *15*, 4546-4554.

III **Photoinduced electron transfer of double-bridged phthalocyanine-fullerene dyads**
Marja Isosomppi, Nikolai V. Tkachenko, Alexander Efimov, Heidi Vahasalo, Johanna Jukola, Pirjo Vainiotalo and Helge Lemmetyinen
Chem. Phys. Lett. **2006**, *430*, 36-40.

IV **Exciplex mediated photoinduced electron transfer reactions of phthalocyanine-fullerene dyads**
Marja Niemi, Nikolai V. Tkachenko, Alexander Efimov, Heli Lehtivuori, Kei Ohkubo, Shunichi Fukuzumi and Helge Lemmetyinen
J. Phys. Chem. A, submitted.

The following papers, where the contribution from the author has been minor, are related to the Thesis:

V **Energy and Electron Transfer in β-Alkynyl-Linked Porphyrin – [60]Fullerene Dyads**

Sean A. Vail, David I. Schuster, Dirk M. Guldi, Marja Isosomppi, Nikolai V. Tkachenko, Helge Lemmetyinen, Amit Palkar, Luis Echegoyen, Xihua Chen and John Z. H. Zhang
J. Phys. Chem. B **2006**, *110*, 14155-14166.

VI **Azobenzene-Linked Porphyrin-Fullerene Dyads**

David I. Schuster, Ke Li, Dirk M. Guldi, Amit Palkar, Luis Echegoyen, Christopher Stanisky, R. James Cross, Marja Niemi, Nikolai V. Tkachenko and Helge Lemmetyinen
J. Am. Chem. Soc. **2007**, *129*, 15973-15982.

Contents

Abbreviations and symbols

A	acceptor
A	absorbance
BET	back-electron transfer
c	constant of parabola curvature
CFD	constant fraction discriminator
CCD	charge carrier device
CS	charge separation, charge-separated
D	donor
DAS	decay associated spectrum
DPV	differential pulse voltammetry
e	electronic charge
E	energy
ET	electron transfer
G	Gibbs free energy
HV^{2+}	1,1-dihexyl-4,4'-dipyridinium diperchlorate
ITO	indium tin oxide
k	rate constant
k_B	Boltzmann's constant
MCA	multichannel analyzer
mma	mean molecular area
n	refractive index
N_A	Avogadro constant
NLC	non-linear crystal
ODA	octadecylamine
OPA	optical parametric amplifier
P	product state
PD	photodetector
PMT	photomultiplier tube
r	radius
R	reactant state

SAM	self-assembled monolayer
SHG	second harmonic generator
T	transient state
T	temperature
TAC	time-to-amplitude converter
TCSPC	time-correlated single photon counting
TEA	triethanol amine
ε	molar absorptivity
ε_0	permittivity of vacuum
ε_{opt}	optical dielectric constant
ε_s	static dielectric constant
κ_{el}	electronic transmission coefficient
λ	reorganization energy
λ_{in}	inner reorganization energy
λ_s	solvent (outer) reorganization energy
ν_n	frequency of passage through transient state
σ^2	mean square deviation

1 Introduction

Developing environmentally sustainable solutions to the increasing energy demand of the world is one of the most important goals of research. The ultimate renewable energy source is the sun, which emits more than enough (120 000 TW [1]) energy onto Earth to cover the current energy need (13 TW [1]) completely. The reason why solar energy is utilized to a much lower degree (2 GW [2]) than possible is the lack of inexpensive and efficient technology for the purpose.

The green plants and bacteria have a better understanding on how to exploit the solar energy than we do. Natural photosynthesis converts solar energy into electrochemical potential, which is used to synthesize high-energy products needed for the growth of the plant. Copying the idea from nature is an intriguing approach to the problem of solar energy conversion. In the natural photosynthetic membranes, arrays of for example chlorophyll molecules are used as antennas to capture sun light and the collected energy is transferred to a reaction centre, where it is used to facilitate the primary electron transfer (ET) reaction generating chemical potential between two chromophores [3-6].

Mimicking nature's complex photosynthesis system in detail is not feasible, but a simpler approach needs to be taken. The essential tasks of the system are light harvesting and electron transfer. Thus the simplest mimic is a dyad molecule consisting of an electron donor (D) and an electron acceptor (A) with at least one of the moieties being able to absorb the light [3-5,7-34]. Efficient ET has been achieved especially in dyad molecules with the donor and acceptor in close contact with each other [3,5,12,15,17-19]. However, the drawback is that in such compounds also the back electron transfer (BET) reaction occurs efficiently. For applications, such as solar cells, the formed charge-separated (CS) state should live long enough to be utilized in the following processes. Nature's solution for this problem is a molecular array, where multi-step ET occurs through several donors and acceptors [3-5,35]. Each step of the reaction occurs efficiently between neighbouring moieties, but in the resulting CS state the charges are separated by a long distance retarding BET. Following this approach secondary electron donors or acceptors can be added to the dyad structure to build molecular triads, tetrads, etc. [3-5,7,8,30,35-42].

In photosynthetic reaction centres the chromophores are held together in a membrane by a protein [3-5,43]. In the artificial systems the close contact between the electron donor and

acceptor is usually achieved with a covalent linker joining the chromophores. A single linker can either be rigid, keeping the donor and acceptor in fixed orientation, or flexible, allowing the choromophores some freedom to move with respect to each other. In either case an advantageous symmetric structure with face-to-face orientation can be difficult to obtain. To realize a more stable, symmetrical dyad structure, two-linker strategies have been developed [11,18,19,44-47]. Such dyads have also been modified to form solid films in which the molecules are oriented controllably [48-50]. This is of special interest for application in photovoltaic devices such as solar cells.

In this study both dyad [III,IV] and triad structures [I,II] were studied. Porphyrins [I,II] and phthalocyanines [III,IV] were selected as the electron donor part of the molecules. Fullerene was used as the acceptor in all the compounds. The two-linker approach was followed in both the dyad and triad molecules. Focus of the study was on detailed determination of the reaction schemes for the compounds after photoexcitation using mainly time-resolved spectroscopic methods [I,III,IV]. The desired efficient ET was achieved in all of the studied compounds and the increase in the CS distance in the triads compared to corresponding dyads resulted in a longer-living CS state. The phthalocyanine-fullerene dyads were found to behave similarly to the previously studied porphyrin- and phytochlorin-fullerene dyads with comparable organization of the donor and acceptor [12,14,15,19,51-53], *i.e.* the ET reaction proceeds via an intramolecular exciplex [IV]. The triad structures were also studied in solid state examining specially the possibility of using the compounds in photovoltaic applications [II]. Enhancement of both photovoltage and photocurrent generation was observed, compared to the corresponding porphyrin-fullerene dyad samples, as was expected on the basis of the study of the triads in solutions [I].

2 Background

2.1 Intramolecular electron transfer

The photoinduced electron transfer processes occurring in the studied donor-acceptor molecules can be interpreted by the classical electron transfer theory developed by Marcus [54]. The theory describes the transition from an initial state (reactant) to a final state (product). In a simple intramolecular photoinduced electron transfer reaction the reactant state is a locally excited state of either the donor (D*−A) or the acceptor (D−A*) and the product state is the charge transfer state, D^+-A^-. In addition to the ET step, the BET reaction from D^+-A^- to the ground state, D−A, can also be explained by the Marcus theory. Furthermore, the theory can give information on the role of certain intermediate states in the ET or BET reactions as will be discussed in the end of this section.

2.1.1 The classical Marcus theory of electron transfer

In Marcus theory, the complex, multidimensional potential energy surfaces of the reactant (R) state and the product (P) state are simplified to parabolas of Gibbs free energy vs. a so-called reaction coordinate (Figure 2.1) [54]. Introducing the reaction coordinate reduces the potential energy surfaces to one dimension, *i.e.* change in the reaction coordinate describes the changes in the nuclear coordinates of the molecule itself and in those of the surrounding solvent [55]. Considering all internal (nuclear) and external (solvent) motions the energy profile along the reaction coordinate is nonparabolic, but near the energy minima the parabolic approximation of the free energy works well [55].

The curvature of the reactant and product parabolas is assumed to be the same [55], so the product surface can be obtained from the reactant by shifting the parabola in reaction coordinate and in energy. The shift in reaction coordinate determines the reorganization energy, λ, and the shift in energy gives the Gibbs free energy of the reaction, $-\Delta G$. The ET reaction takes place at the transition (T) state, where the reactant and product parabolas intersect, *i.e.* at the point where the reactant and product have the same configuration of nuclear coordinates [55]. Thus, for ET to take place, the reactant must distort from its equilibrium by the activation energy, E_A. Using the notations of Figure 2.1 the reactant and product parabolas are

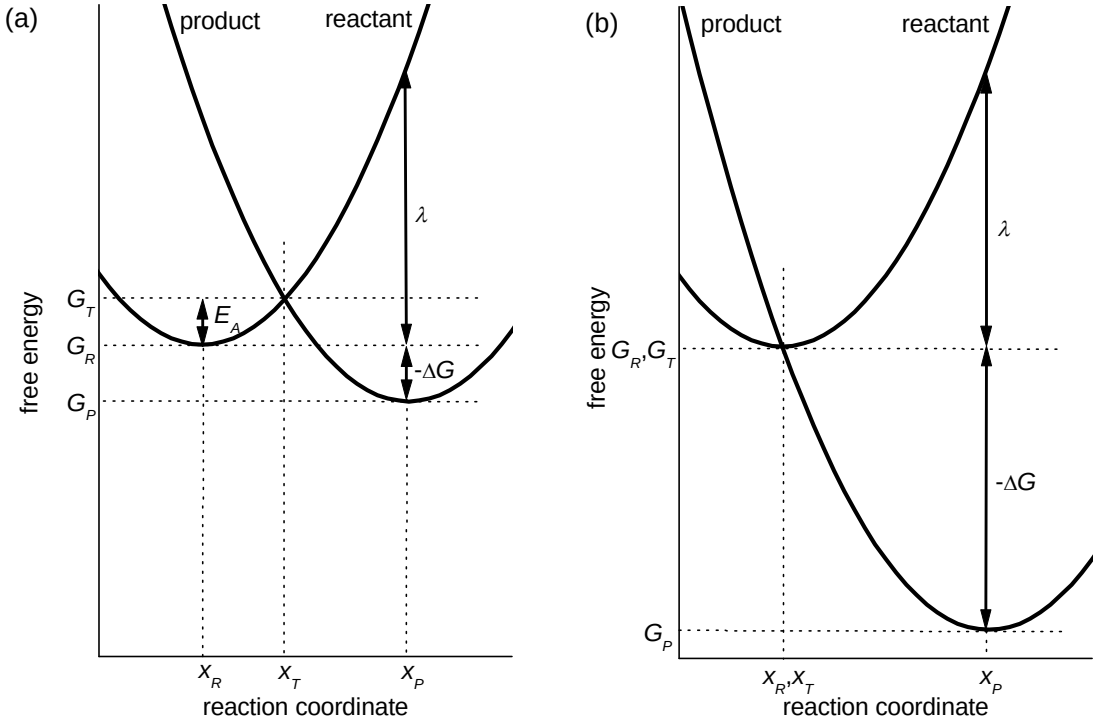

Figure 2.1. Gibbs energy surfaces of the reactant and product states with (a) $-\Delta G < \lambda$ (normal region) and (b) $-\Delta G = \lambda$ (maximum k_{ET}).

$$E_R(x) = c(x - x_R)^2 + G_R$$
$$E_P(x) = c(x - x_P)^2 + G_P \qquad (1)$$

Coefficient c describes the parabola curvature and is the same for the reactant and product states as it was assumed above. Introducing $\Delta x = x_P - x_R$ and $\Delta G = G_P - G_R$ one can solve the reaction coordinate of the transient state from the intersection of the two parabolas as

$$x_T = \frac{\Delta G}{2c\Delta x} + \frac{x_R + x_P}{2}. \qquad (2)$$

The reorganization energy, λ, is given as

$$\lambda = E_R(x_P) - G_R = c\Delta x^2, \qquad (3)$$

and the activation energy, E_A, of the ET reaction becomes

$$E_A = G_T - G_R = \frac{(\Delta G + \lambda)^2}{4\lambda}. \quad (4)$$

According to classical transition state theory the population at the transient state follows the Boltzmann distribution and the rate constant for ET is [43,55]

$$k_{ET} = \kappa_{el} \nu_n \exp\left(-\frac{E_A}{k_B T}\right), \quad (5)$$

where κ_{el} is the electronic transmission coefficient, ν_n is the frequency of passage through the transition state, k_B is the Boltzmann constant, and T is the temperature. In the classical Marcus theory κ_{el} is usually estimated to be unity and ν_n is of the same order of magnitude as molecular vibrational motion (10^{13} s^{-1}) [55]. Inserting eq. 4 to eq. 5 gives the classical Marcus equation

$$k_{ET} = \kappa_{el} \nu_n \exp\left[-\frac{(\Delta G + \lambda)^2}{4\lambda k_B T}\right]. \quad (6)$$

The reorganization energy can be presented as a sum of two contributions: the solvent independent inner term, λ_{in}, and the outer term or the solvent reorganization energy, λ_s [54,55]. The inner term arises from the structural differences of the molecule in the reactant and product states and it can be expected to be fairly small especially for the big, rigid, and highly symmetrical molecules as the ones used in this study [55]. The outer term corresponds to the differences in the orientation and polarization of the solvent molecules around the studied molecule in the reactant state and in the product state [55]. Treating the solvent as a dielectric continuum and approximating the electron donor and acceptor as spherical the solvent reorganization energy is [54,55]

$$\lambda_s = \frac{e^2}{4\pi\varepsilon_0}\left(\frac{1}{2r_D} + \frac{1}{2r_A} - \frac{1}{r_{DA}}\right)\left(\frac{1}{\varepsilon_{opt}} - \frac{1}{\varepsilon_s}\right), \quad (7)$$

where e is the charge transferred in the reaction, *i.e.* one electron charge, ε_0 is the vacuum permittivity, ε_{opt} (= n^2, where n is the refractive index of the solvent) and ε_s are the optical and

static dielectric constants of the solvent, r_D and r_A are the radii of the donor and the acceptor, respectively, and r_{DA} is the centre-to-centre distance between the donor and the acceptor.

As mentioned above, the electronic transmission coefficient, κ_{el}, or the probability that transition from the reactant to the product parabola occurs at the transition state, is assumed as unity in the classical theory. For ET reactions with $\kappa_{el} \ll 1$ a quantum mechanical treatment of the Marcus theory must be used. The quantum mechanical treatment takes into account the probabilities of electron and nuclear tunnelling between the reactant and product states. [55]

2.1.2 Interpreting electron transfer reactions

Taking a careful look at equations 6 and 7 and at Figure 2.1 one can understand the factors influencing the rate of ET.

1. The exponential term of eq. 6 reveals that the maximum ET rate is achieved in a condition $-\Delta G = \lambda$ as illustrated in Figure 2.1b. When $-\Delta G < \lambda$, k_{ET} increases as $-\Delta G$ increases, *i.e.* as the reaction becomes more exergonic. This situation, the normal region, is illustrated in Figure 2.1a. When $-\Delta G > \lambda$, k_{ET} starts to decrease as $-\Delta G$ increases. This is the so-called inverted region [43,54,55].
2. Similarly, the exponential term of eq. 6 also shows that decreasing λ for a given $-\Delta G$ results in higher k_{ET}, but only to a certain limit after which k_{ET} starts to decrease again (inverted region). From eq. 7 one notices that in the same solvent λ_s becomes smaller with increasing r_D or r_A and with decreasing r_{DA} [54,6]. In other words, the ET rate can be increased to a certain extent by increasing the sizes of the donor and acceptor and by decreasing the distance between them.
3. Decreasing solvent polarity, *i.e.* the static dielectric constant ε_s in eq. 7, decreases the reorganization energy and thus increases k_{ET} to some extent [54]. However, in a very non-polar solvent ET may again be pushed to the inverted region and slowed down (Figure 2.2).

The Marcus theory can be applied just as well to the BET reaction. Figure 2.2 shows the Gibbs energy profiles of a simple photoinduced ET-BET reaction in a donor-acceptor dyad. The states involved in the reaction are the ground state, D−A, the locally excited state of the donor, D*−A, and the CS state, D^+-A^-. The curvature of the parabola is the same for all the states and the energy minimum of D*−A is assumed to be at the same reaction coordinate as that of D−A. Thus, D*−A is shifted from D−A only by the excited state energy, which is experimentally available from the absorption and emission spectra of the compound. The energy shift of D^+-A^-

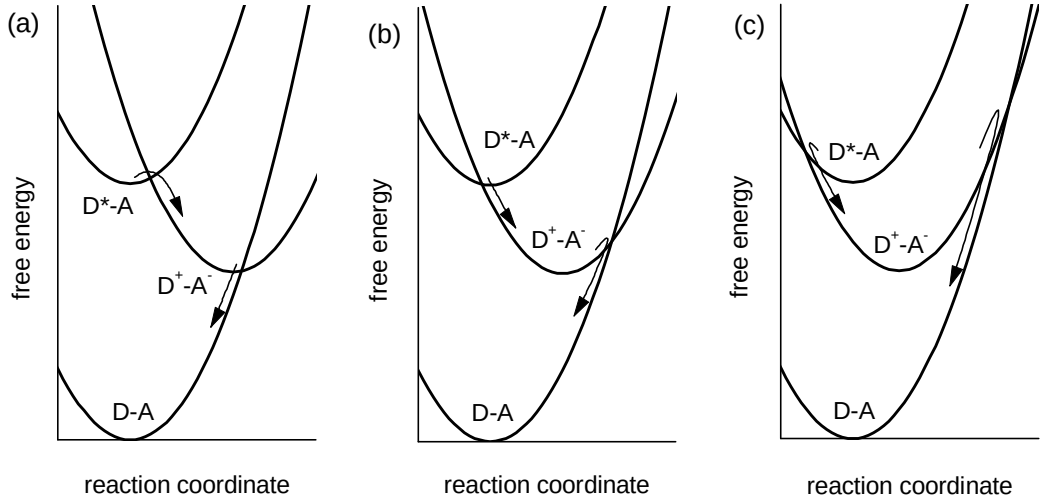

Figure 2.2. Gibbs free energy surfaces for ET and BET reactions with different reorganization energies, λ. (a) High λ results in ET in the normal region and in relatively fast BET. (b) Decreasing λ increases k_{ET} and pushes BET to the inverted region. (c) Further decrease in λ slows BET further, but also ET is pushed to the inverted region.

compared to D−A can be estimated with electrochemical methods (see section 3.4) and the shift in the reaction coordinate depends on the reorganization energy, λ (see eq. 3 and eq. 7). The schemes in Figure 2.2 are otherwise the same, but λ becomes lower from (a) to (c). It is clear that λ has an influence on the rates of both the ET and the BET reaction, but the influence on BET is more pronounced. This can be rationalized considering the same molecule in different solvents, *i.e.* varying λ_s (or the parabola curvature *c*, see eq. 3). For ET reactions of neutral donor and acceptor, both $-\Delta G$ and λ of ET decrease with decreasing solvent polarity, as a result of decreased stabilization of the charge-separated state. Neglecting variations in the solvent refractive index (*i.e.* in ε_{opt}, see eq. 7), the decrease in $-\Delta G$ and λ is approximately equal in magnitude and $\Delta G + \lambda$ (eq. 6) should be approximately independent of solvent [56]. Instead in a BET reaction a neutral species is formed from a CS state. Also for BET λ decreases as the solvent polarity decreases, but $-\Delta G$ increases. Thus, $\Delta G + \lambda$ decreases (becomes more negative in the inverted region) and the BET process is pushed further into the inverted region. [56]

The Marcus theory works well for the one step ET and BET reactions described above. However, more complex reactions with intermediate steps can be difficult to interpret quantitatively with the 1-dimensional model. Still, some qualitative insight into the role of the

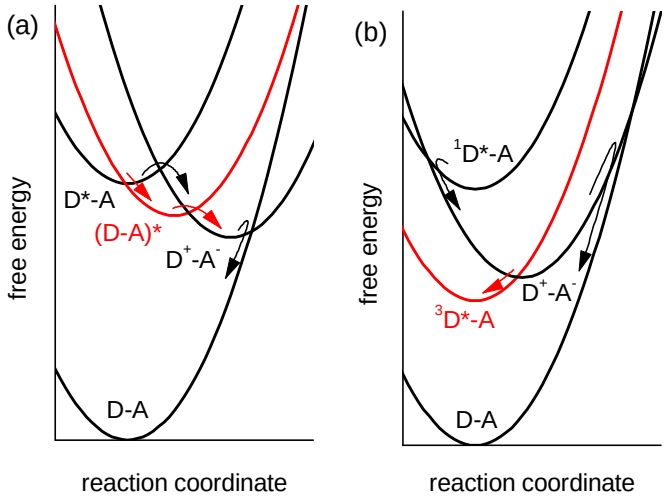

Figure 2.3. Intermediate states (given in red) in the ET and BET reactions. (a) An exciplex state, (D−A)*, can accelerate the ET reaction by lowering the activation energy. (b) The CS state, $D^{+}-A^{-}$, can transform into an intermediate state, such as an excited triplet state of the donor, $^{3}D^{*}-A$, instead of relaxing directly to the ground state.

intermediates can be gained by using the simple parabolic energy profiles [57]. Two examples of possible intermediates in a photoinduced ET reaction of a D−A dyad are presented in Figure 2.3.

In Figure 2.3a the ET reaction proceeds via an intramolecular exciplex state, (D−A)*. The exciplex is a complex that exists only in an excited state [58]. It is a common excited state of the donor and the acceptor, *i.e.* a state where the electron is delocalized on the molecule. For some compounds the exciplex shows strong emission [12,14,19,29,32,56,58-61] and for such compounds it is possible to estimate both $-\Delta G$ and λ of the D*−A → (D−A)* reaction [12,14,19,32,59]. As seen in the figure, the exciplex can lower the overall activation energy of the ET reaction and increase k_{ET} [14,57].

There can also be an intermediate step in the BET reaction. In Figure 2.3b the intermediate is a triplet state of the donor, $^{3}D^{*}-A$. Since the difference between the singlet excited state of the donor, $^{1}D^{*}-A$, and $^{3}D^{*}-A$ is only the spin of one electron, it is assumed here, that the triplet state has a similar structural configuration as the singlet excited state, $^{1}D^{*}-A$ (and the ground state, D−A), or the same reaction coordinate of the energy minimum. The spin forbidden transition to the triplet state is possible for big molecules, such as the ones in this study, and relaxation of $D^{+}-A^{-}$ to $^{3}D^{*}-A$ may become a significant process, if BET directly to D−A is far in the inverted region, like illustrated in Figure 2.3b.

2.2 Donor-acceptor compounds

Donor-acceptor compounds serve as artificial models of the photosynthetic reaction centre. Careful design of such molecules must take into account the following factors arising from the electron transfer theory described in the previous section:

1. appropriate redox potentials of the donor and acceptor to enable ET;
2. suitable size and symmetry of the donor and acceptor to optimize λ and thus k_{ET} and k_{BET};
3. light harvesting ability of at least one of the chromophores, *i.e.* strong enough absorption at a wavelength where excitation can be carried out;
4. suitable excited state energy of the light harvesting chromophore, *i.e.* negative free energy of ET from the excited state;
5. mutual orientation and distance of the chromophores, *i.e.* control of λ and thus k_{ET} and k_{BET}.

2.2.1 Porphyrins, phthalocyanines and fullerenes

Porphyrins (porphine as an example in Figure 2.4) and phthalocyanines are models for the less stable and less synthetically tractable chlorophylls, which are common electron and energy donors in natural photosynthesis [4]. All of these macrocycles consist of four conjugated pyrrole rings. In phthalocyanines the pyrrole units are extended to isoindoles, which are joined via aza bridges instead of methynes as in porphyrins (Figure 2.4). The porphyrin and phthalocyanine molecules having two imine hydrogens inside the macrocycles, such as the ones in Figure 2.4, are called “free-base” structures. Porphyrins and phthalocyanines are able to complexate various metals and many properties of the compounds can be altered by central metal substitution [62]. In addition, porphyrins and phthalocyanines can be modified with peripheral side groups to the macrocycles [62]. Properties that can be influenced are e.g. solubility, redox potentials and

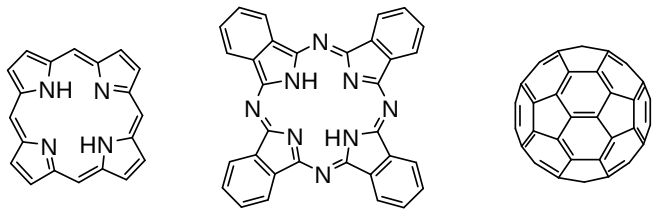

porphine phthalocyanine C_{60} fullerene

Figure 2.4. Structures of porphine, phthalocyanine and C_{60} fullerene.

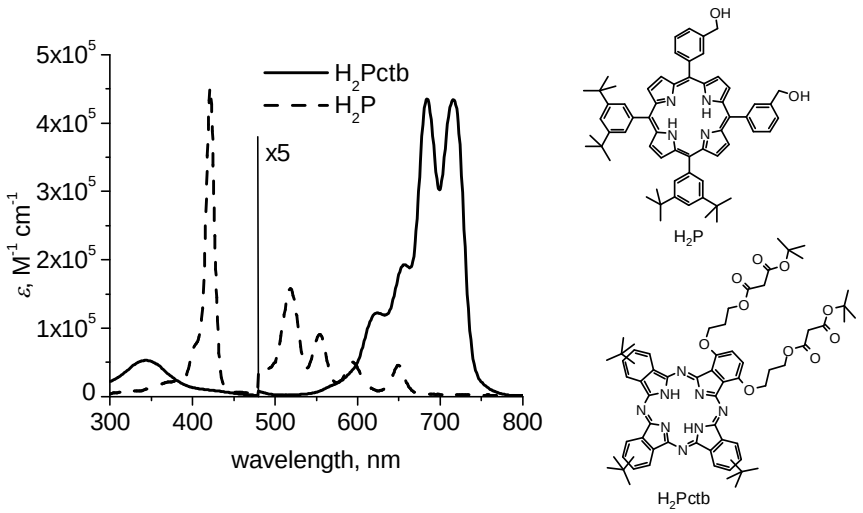

Figure 2.5. Absorption spectra in toluene for free-base porphyrin [I] and phthalocyanine [IV] reference compounds used in the study.

excited state energies, which in turn affect the photophysical behaviour of the chromophores in donor-acceptor systems.

Absorption spectra of a porphyrin and a phthalocyanine reference compound used in this study are presented in Figure 2.5. The absorption spectra of both porphyrin and phthalocyanine show two characteristic absorption regions with high molar absorptivity (ε): the Soret band at roughly 430 nm or 350 nm for porphyrin and phthalocyanine, respectively, and the Q bands around 500-650 nm for porphyrin and at 600-750 nm for phthalocyanine. The Soret band accounts for the transition of the chromophore to its second excited singlet state while the Q bands originate from transitions to the first excited singlet state. It can be seen in Figure 2.5 that compared to porphyrins phthalocyanines have stronger absorbance in the spectral region 550-800 nm matching better with the spectrum of white light. This makes phthalocyanines more attractive chromophores in solar energy conversion.

Fullerenes are even-numbered clusters of carbon atoms in the range of C_{30}-C_{100} [63,64]. The most stable structure of the fullerenes is the one consisting of 60 carbon atoms, *i.e.* C_{60} or buckminsterfullerene (Figure 2.4) [64]. C_{60} is a polyhedron with 12 pentagonal and 20 hexagonal faces. Each carbon atom of the C_{60} ball is equal to the others and the conjugation extends throughout the surface of the ball [63]. The symmetry of C_{60} leads to its unique properties as an electron acceptor in donor-acceptor compounds: the reorganization energies (see section 2.1) of the C_{60} containing donor-acceptor dyads are significantly lower compared to dyads with otherwise similar structure but different acceptor moieties [65-67]. Since C_{60} was used as the electron acceptor in this study, the term “fullerene” refers to C_{60} in the Thesis.

Porphyrin and phthalocyanine can act as either electron donors or acceptors in their excited state depending on the environment, *i.e.* on the chromophores they are coupled to [62]. For example, the first oxidation potentials of the porphyrin (**H_2P**) and phthalocyanine (**H_2Pctb**) reference compounds used in this study (Figure 2.5) are +1.0 eV and +0.6 eV, respectively, and the first reduction potentials are −1.2 eV and −0.8 eV, all measured in benzonitrile. The first reduction potential of fullerene in benzonitrile is −0.6 eV [68] making it a suitable electron acceptor when coupled with either porphyrin or phthalocyanine as a donor. The ability of fullerene to accept electrons is not limited to just one, but it can be reduced up to six times [69].

2.2.2 Dyads and triads

The simplest molecule capable of intramolecular photoinduced electron transfer is a donor-acceptor dyad, which is able to absorb light efficiently. The absorbing moiety can be either the donor or the acceptor. Porphyrin-fullerene [4,8-16,19] and phthalocyanine-fullerene [20-26,68] dyads have been widely studied, because of the advantageous properties of the chromophores discussed in section 2.2.1. Since porphyrin and phthalocyanine exhibit much stronger absorption in the visible wavelength range compared to fullerene, they are the moieties usually excited in the studied dyads. For example, irradiating a phthalocyanine-fullerene dyad molecule with light at the phthalocyanine Q bands (see Figure 2.5) excites the phthalocyanine moiety exclusively. The first singlet excited state of phthalocyanine has a higher energy (1.7 eV for the **H_2Pctb** reference shown in Figure 2.5) than the CS state in a phthalocyanine fullerene dyad (1.2 eV for dyad **H_2Pc-C_{60}tb** used in this study, see Figure 3.1 for the molecular structure). Thus, the phthalocyanine unit promoted to its singlet excited state can donate an electron to fullerene and the CS state is formed in an exergonic reaction.

Due to the short CS distance in the donor-acceptor dyads, both the ET and the BET reactions are often rapid. Slowing down BET is desired, because a longer living CS state can be more easily utilized in further applications of the compounds. Expanding the length of the linker joining the donor and acceptor results in a longer-living CS state, but it also slows down the ET reaction lowering the quantum yield of the CS state [70,71]. A strategy adopted from nature is dividing the formation of the final CS state in several short distance ET reaction steps. Adding a secondary electron donor or acceptor to the donor-acceptor pair the dyad can be extended to a triad, where a relatively long-living complete CS state is formed in two fast ET reaction steps [3-5,7,8,35,37,39,41,42].

As discussed in section 2.1 the centre-to-centre distance of the donor and acceptor is an important factor affecting the reorganization energy and the ET rate. Particularly fast ET rates

have been observed for compounds with the donor and acceptor moieties in close, face-to-face contact, where the orbitals of the donor and acceptor overlap with each other [5,19,72]. Such orientation can be achieved for example by joining the donor and acceptor symmetrically with two covalent linkers [11,18,19,45-47].

3 Materials and methods

All the spectroscopic measurements were carried out at least in two different solvents, *i.e.* in benzonitrile and toluene representing polar and non-polar environments, respectively.

3.1 Compounds

Two kinds of donor-acceptor molecules were studied for this Thesis: porphyrin-porphyrin-fullerene triads [I,II] and phthalocyanine-fullerene dyads [III,IV]. All the studied compounds were synthesized at the Department of Chemistry and Bioengineering, Tampere University of Technology. Molecular structures of the studied compounds are presented in papers I-IV. Example structures of triads (**P_2t9P_1C** and **ZnP_2t9P_1C**, paper I) and dyads (**H_2Pc-C_{60}tb** and **ZnPc-C_{60}tb**, paper IV) are given in Figure 3.1. The two-linker strategy was utilized in the design of all the studied compounds: the donor and acceptor moieties are attached with a pair of molecular chains keeping the structures fixed and oriented.

The phthalocyanine-fullerene compounds are simple mimics of nature's reaction centre, *i.e.* they consist of a phthalocyanine moiety as an electron donor and a fullerene moiety as an

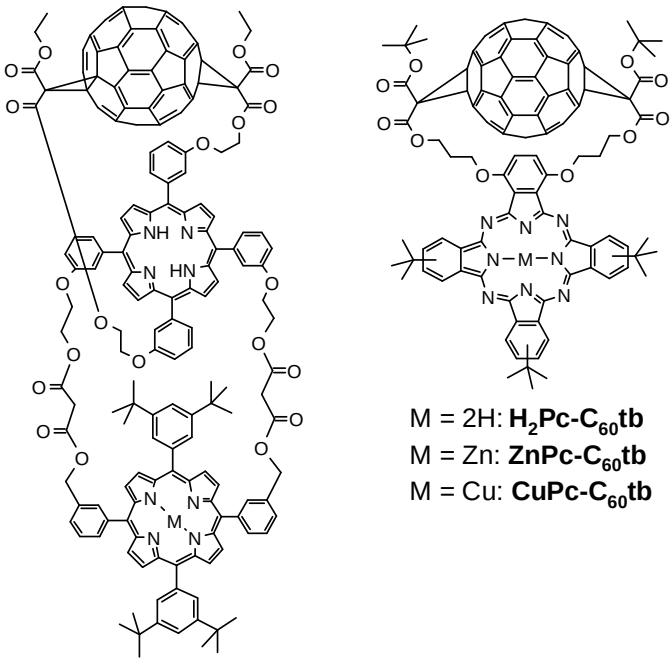

Figure 3.1. Molecular structures of **P_2t9P_1C**, **ZnP_2t9P_1C**, **H_2Pc-C_{60}tb**, **ZnPc-C_{60}tb** and **CuPc-C_{60}tb**.

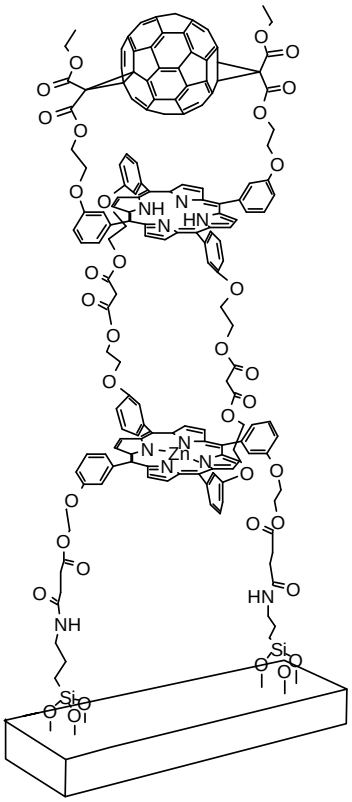

Figure 3.2. Idealized structure of a porphyrin-porphyrin-fullerene triad SAM on glass substrate.

electron acceptor. Effect of the central metal of the phthalocyanine ring was studied with a series of three dyads (Figure 3.1) with otherwise the same structure but altering metal substitution. Also different attachment positions of the linkers on the phthalocyanine moiety were studied. [III,IV]

In the porphyrin-porphyrin-fullerene triads another porphyrin moiety is attached to the free-base porphyrin-fullerene dyad to act as a secondary electron donor. Distance dependence between the two porphyrin moieties and metal substitution on the second porphyrin unit was examined with three different triad structures. [I]

In order to investigate the possibility of applying the compounds studied in solutions as solid state photovoltaic devices, successive self-assembled monolayers (SAMs) of Zn porphyrins and free-base porphyrin-fullerene dyads were deposited on indium tin oxide (ITO) covered glass substrates to obtain organized porphyrin-porphyrin-fullerene triad layers. Like for the triad structures studied in solutions, positions of the attaching linkers were altered to obtain two different orientations of the ZnP layer: the linkers to the substrate (and to the following dyad layer) are in the adjacent (*cis*-structures) or opposite (*trans*-) phenyl groups of the porphyrin unit. Idealized structure of the ***trans*-triad** sample is presented in Figure 3.2. In reality there was more than one Zn porphyrin per each porphyrin-fullerene dyad in the samples, because the Zn

porphyrin layer attached first to the substrate was very densely packed. Structures of the other SAM samples and the deposition procedure are presented in paper II.

3.2 Steady-state absorption and emission spectroscopy

Spectroscopic steady-state measurements were carried out for all studied compounds before time-resolved measurements to determine the wavelengths where the individual chromophores and the dyad and triad compounds absorb and emit. Based on the steady-state absorption spectra it was possible to select the excitation wavelength in the time-resolved absorption or fluorescence measurements so, that a certain chromophore of the molecule could be specifically excited. The absorption spectrum was also referred to, when interpreting the time-resolved absorption measurements, in which the change in absorption relative to the ground state absorption was detected. Furthermore, based on the steady-state fluorescence spectra the fluorescence decays of specific choromophores of the molecules were followed at certain wavelengths.

In addition to being a complementary tool for the time-resolved spectroscopic studies, the steady-state methods as such reveal interactions between the chromophores of the dyads and triads. The absorption spectra of all dyads and triads showed slight decrease in molar absorptivity and broadening of the absorption bands compared to the absorption spectra of the individual chromophores [I,III,IV]. The characteristic intense emission of the porphyrin or phthalocyanine moieties of the dyad and triad compounds was efficiently quenched by the fullerene moiety [I,III,IV]. The more efficient quenching observed in polar solvent compared to non-polar solvent indicated that the porphyrin or phthalocyanine singlet excited state emission was quenched due to electron transfer to fullerene. For the porphyrin-porphyrin-fullerene triad compounds characteristic porphyrin-fullerene exciplex emission was clearly observed in the steady-state measurements in non-polar solvent [I].

3.3 Time-resolved spectroscopy

Time-resolved spectroscopy was used to determine the photoinduced reaction schemes of the dyad and triad molecules [I,III,IV]. The measurements allowed to identify the transient species of the reactions and provided rate constants for the different steps. In the transient absorption measurements a laser pulse at an appropriate wavelength is used to excite the sample molecules and continuous light or a light pulse is used to detect absorption of the formed excited state. Also in the time-resolved fluorescence measurements a short pulse of light is used for excitation and the decay of the excited state emission is monitored at a certain wavelength. Two methods with

different time scales were used for both absorption and emission measurements: pump-probe and up-conversion for the fastest processes and flash-photolysis and time-correlated single photon counting for longer-living species.

3.3.1 Pump-probe

Scheme of the pump-probe instrument used for transient absorption measurements in the picosecond time-scale is presented in Figure 3.3. The excitation source (not shown in the scheme) is a Ti:sapphire laser generating 100 fs pulses at ~800 nm. The beam at the laser fundamental frequency is split in two. A part of the beam goes through a second harmonic generator (SHG) forming the excitation (pump) pulses and the other part is passed through a water cuvette generating white continuum for detecting (probe) the absorbance changes in a wide spectral region. The probe beam is further split in two: a signal beam and a reference beam, which are both focused on the sample cuvette. The pump beam is passed through a delay line with a moving right angle reflector, which is used to tune the optical path length of the pump pulse relative to the probe pulse, and focused on the signal beam in the sample cuvette. Depending on the position of the moving mirror on the delay line the pump pulse arrives at the sample at a certain time before the probe pulse and absorption of the sample at a known time after the excitation is measured. By scanning the moving mirror through the entire delay line one can detect changes in absorption starting from before the excitation (at negative delay times) to the upper limit of 1.2 ns after excitation, which is due to the limited length of the delay line.

The second harmonic of the titanium-sapphire laser fundamental was mostly used for sample excitation and it was adjusted in the range 390-425 nm depending on the absorption of the

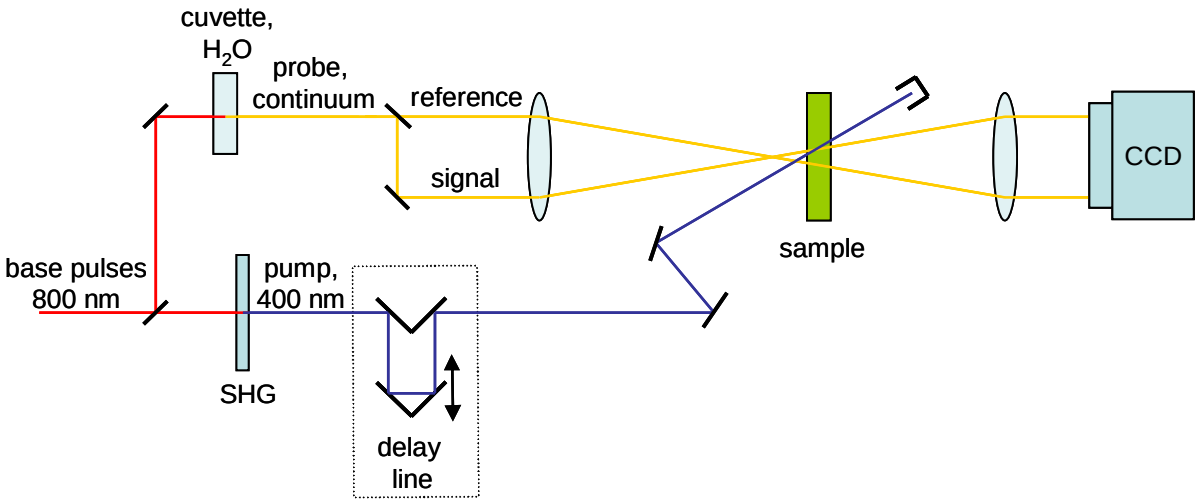

Figure 3.3. Simplified scheme of the pump-probe method [73].

measured sample. To obtain specific excitation of either free-base or Zn porphyrin in the triad **ZnP_2t9P_1C** (Figure 3.1) an optical parametric amplifier (OPA) was used instead of SHG. With OPA the excitation wavelength was adjusted to 515 nm (free-base porphyrin) or to 550 nm (Zn porphyrin). [I]

From the detected changes in absorption it is possible to identify transient species formed after the sample excitation. Thus, the time-resolved absorption measurements give direct information about the scheme of the photoinduced reaction. The raw data obtained from the measurements consists of the differential transient spectra at different delay times. From this primary data transient absorption decay curves at different wavelengths can be drawn. In the data analysis procedure the decay curves are fitted globally to a sum of exponentials

$$\Delta A(\lambda,t) = \sum a_i(\lambda)\exp\left(-\frac{t}{\tau_i}\right), \tag{8}$$

where a_i are the amplitudes and τ_i are the lifetimes of the components. The number of components needed for a reasonable fitting of the data should give the number of transient species in the reaction and rate constants of the reaction steps can be calculated from the corresponding lifetimes. The amount of the components, or the exponentials, was decided based on the improving fit quality when increasing the exponentials one by one. The quality was considered as improved, if the mean square deviation, σ^2, improved by more than 10 %. For example, if σ^2 of a bi-exponential fit compared to that of a mono-exponential one improved more than 10 %, it was concluded that at least two exponents were needed for a reasonable fitting. Further on, if a tri-exponential fitting improved σ^2 by less than 10 %, the bi-exponential fitting was considered as sufficient to describe the data.

The transient absorption results in papers I, III and IV are mainly presented as so-called decay component spectra, where the amplitudes of the components from the fitting are plotted at each wavelength. Time-resolved spectrum at any given time can be calculated from eq. 8 and if the reaction scheme is known, spectra of the different transient species of the reaction can be drawn as well.

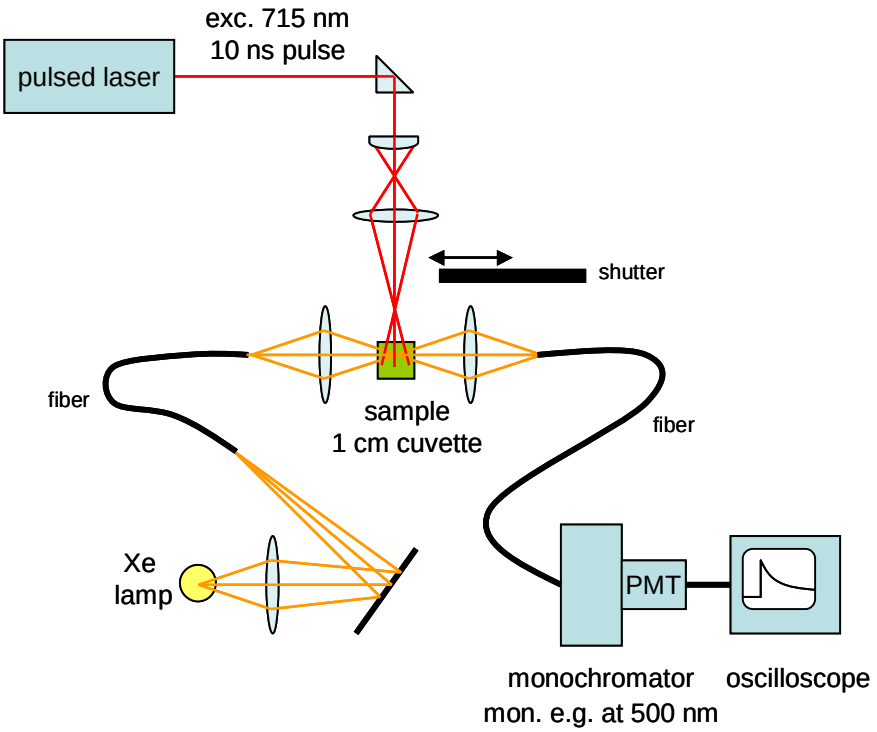

Figure 3.4. The flash-photolysis measurement system used in the study.

3.3.2 Flash-photolysis

The measurement scheme of the flash-photolysis method used to study time-resolved absorption in microsecond time-scale is presented in Figure 3.4. The method is similar to the pump-probe method, but continuous light is used for the monitoring instead of the light pulse used in the pump-probe. 10 ns pulses from a tunable Ti:sapphier laser (pumped by second harmonic of Nd:YAG laser) are used for excitation. The signal is recorded with a digitizing oscilloscope at one wavelength at a time. The excitation wavelengths used in the present study were 715 nm and 400 nm (second harmonic). The samples were deoxygenated by nitrogen bubbling for 20 min prior to the measurements and a nitrogen flow was maintained on the surface of the solution during the measurements to inhibit triplet state quenching by molecular oxygen.

The data analysis procedure for the results of the flash-photolysis measurements is the same as described for pump-probe in section 3.3.1.

3.3.3 Up-conversion

The same femtosecond Ti:sapphire laser utilized in the pump-probe measurements was used to measure time-resolved fluorescence with the up-conversion method. In the up-conversion

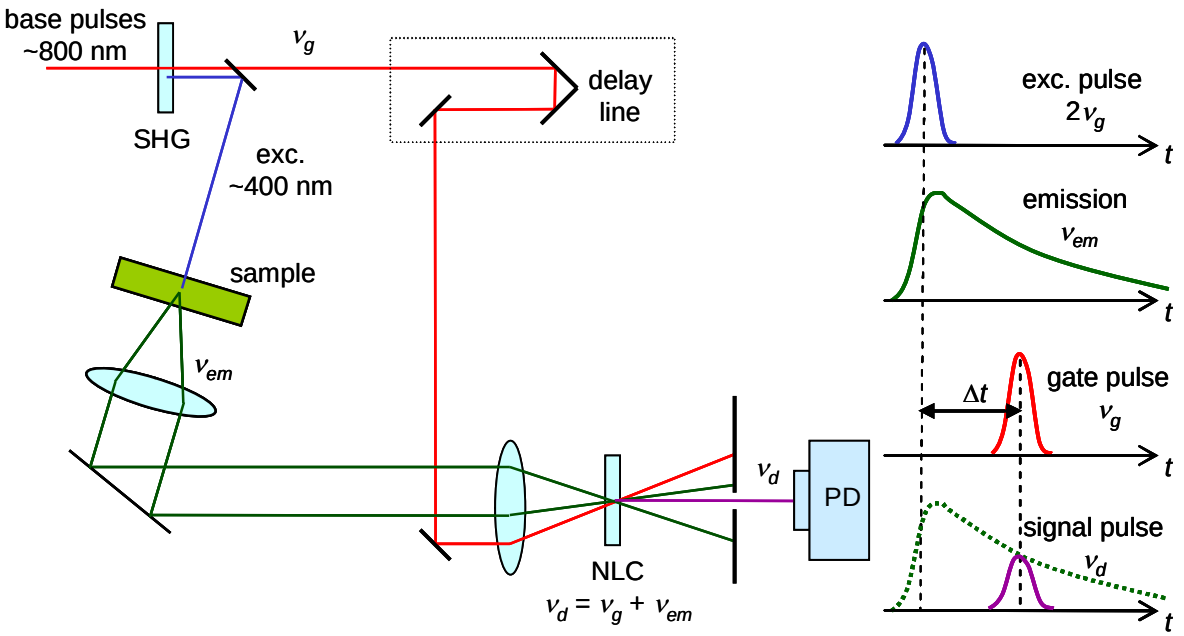

Figure 3.5. Simplified scheme of the up-conversion method for fluorescence decay measurements [73].

measurements (Figure 3.5) the second harmonic of the 100 fs laser pulse is used for sample excitation and emission from the sample is focused to a non-linear crystal (NLC), where it is mixed with the so-called gate pulse, which is the laser fundamental. The gate pulse picks a narrow time interval of the sample emission and the signal is measured at a sum frequency (ν_d) of the gate (ν_g) and the selected emission frequency (ν_{em}) of the sample, *i.e.* $\nu_d = \nu_g + \nu_{em}$. The method is called up-conversion because the signal is not detected at the frequency of sample emission, ν_{em}, but at a frequency shifted by ν_g. The gate pulse is passed through a delay line similar to that used in the pump-probe setup so that it arrives at NLC at a desired time after sample excitation. The detection system measures the light intensity at ν_d, which is proportional to the emission intensity at a certain time after excitation and scanning through the delay line the emission decay curve of the sample can be detected starting from before the excitation (negative delay time) to 1.2 ns after the excitation (limited by the delay line length).

In this study the up-conversion measurements were carried out to determine the lifetimes of the first excited singlet states of porphyrins and phthalocyanines in the dyads and triads [I,III,IV]. The excitation wavelength was typically 410-425 nm, promoting the porphyrin or phthalocyanine chromophore of the molecule to the second excited singlet state, which rapidly transforms into the emitting first excited singlet state via internal conversion. The monitoring wavelength was selected so that emission from a desired chromophore of the dyad or triad compound was followed. For example in the triad compound **ZnP_2t9P_1C** both the Zn porphyrin

and the free-base moiety of the compound absorb at the excitation wavelength, but by selecting 600 nm as the monitoring wavelength, it was possible to follow emission specifically from the Zn porphyrin [I].

The emission decay curves obtained from the up-conversion measurements are fitted exponentially just as the transient absorption decay curves (eq. 8).

3.3.4 Time-correlated single photon counting

Fluorescence decays of the samples in the nanosecond and sub-nanosecond time scales were measured using a time-correlated single photon counting (TCSPC) system (Figure 3.6). The pulsed light from a laser is split in two and a part of it is used to excite the samples and another part is used for triggering ("start" pulse). Emission from the sample is directed to a photomultiplier tube (PMT), where each detected photon creates an electric pulse (single photon counting). The triggering light pulse creates an electric pulse at the photodiode (PD) and both the triggering pulse and the pulse from PMT are directed to the time-to-amplitude converter (TAC) via the constant fraction discriminators (CFD), which equalize the incoming pulses in shape and amplitude. In TAC the triggering "start" pulse starts operation of a linearly rising voltage generator and the pulse from the PMT (first detected emission photon) stops the generator ("stop" pulse). The output voltage of the generator depends on the time delay between the "start"

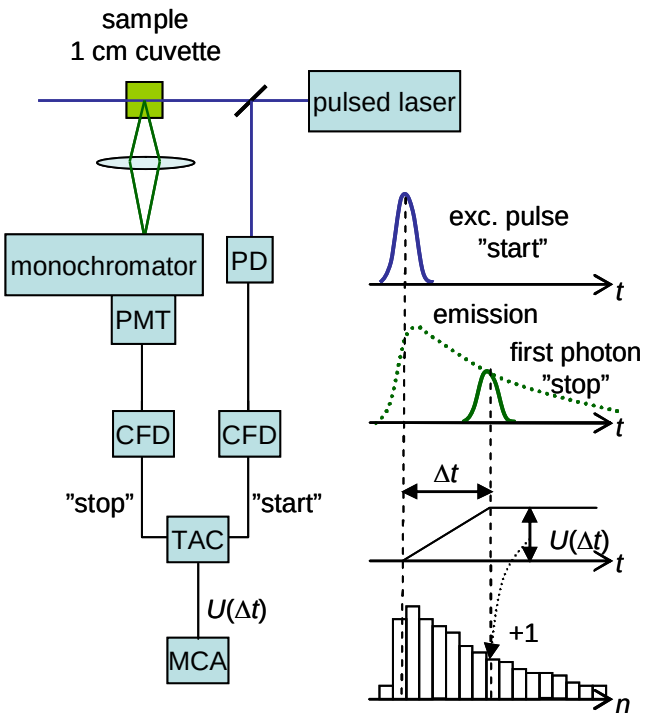

Figure 3.6. Scheme of the TCSPC measurement system [73].

and “stop” pulses. Multichannel analyzer (MCA) analyzes the voltage output of the generator. The MCA memory is divided into channels that correspond to voltage intervals and the voltage from TAC increases the value of the matching channel by one. Since the voltage from TAC is proportional to the delay time, the MCA channels refer to time intervals and the decay profile of the sample is recorded by counting the photons arriving at each time delay after excitation.

The time resolution of the TCSPC measurements in this study was about 60-100 ps (FWHM of the instrument response function). TCSPC was mainly used to determine the lifetimes of the singlet excited states of the reference compounds [I,IV], because most processes in the dyad and triad compounds occur in a faster time scale and for those up-conversion method described in section 3.3.3 is more suitable. For the porphyrin-porphyrin-fullerene triads TCSPC was a useful method also for determining the lifetime of the long-living emitting exciplex state [I].

The TCSPC data is analyzed the same way as the data from the other time-resolved methods (see previous sections). A TCSPC measurement is considerably faster to carry out than an up-conversion measurement making it more convenient for measuring a wider spectral region for a specific sample. The decay curves at different wavelengths can be fitted globally like the transient absorption decay curves (see section 3.3.1) to obtain emission decay component spectra or decay associated spectra (DAS). In this study DAS were measured with TCSPC to resolve the different emitting species of the porphyrin-porphyrin-fullerene triads, in which the emission of the free-base porphyrin first excited singlet state overlaps with that of the exciplex [I].

3.3.5 Comparison of the time-resolved methods

The four different time-resolved methods described in the previous sections are compared in Table 3.1. The use of the different methods provided the possibility to study the processes in different time scales. Table 3.1 also lists the wavelengths used for excitation and monitoring in the different instruments.

Table 3.1. Comparison of the time-resolved methods used in the study.

method	**time resolution**	**time upper limit**	**excitation wavelength**	**monitoring range**
pump-probe	150 fs	> 1.2 ns	390-425 nm, 515 nm, 550 nm	400-1100 nm
flash-photolysis	10 ns	> 10 s	715 nm, 400 nm	400-850 nm
up-conversion	150 fs	> 1.2 ns	400-425 nm	600-740 nm
TCSPC	60-100 ps	> 200 ns	405 nm, 590 nm	600-850 nm

3.4 Differential pulse voltammetry

Differential pulse voltammetry (DPV) was used to estimate the energies of the CS states of the dyads and triads [I,III,IV]. The first oxidation potentials, $E^0(D^+/D)$, of the donor porphyrins and phthalocyanines and the first reduction potential, $E^0(A/A^-)$, of the acceptor fullerene in the dyad and triad compounds were measured with DPV using Ag/AgCl as pseudo-reference electrode. Tetra-*n*-butylammonium tetrafluoroborate in benzonitrile was used as the supporting electrolyte and the measurements were carried out in a nitrogen flow. After measuring the background, benzonitrile solution of the sample was added to the electrochemical cell. The concentrations of the samples in the cell were 0.3-0.8 mM. Finally, the measurements were repeated after adding ferrocene/benzonitrile as an internal reference. The measurements were carried out in both directions: towards the positive and negative potential. The reduction and oxidation potentials were calculated as an average of the two scans.

The energy of a CS state can be calculated using the Rehm-Weller equation [74] as

$$E_{cs} = E^0\left(D^+/D\right) - E^0\left(A/A^-\right) - \frac{e^2}{4\pi\varepsilon_0\varepsilon_s r_{DA}}. \quad (9)$$

The final term on the right hand side of eq. 9 accounts for the attractive Coulombic forces pulling the charged donor and acceptor (approximated as point charges) closer together, *i.e.* lowering the energy of the CS state [74]. For the studied phthalocyanine-fullerene dyads r_{DA} was estimated to be 13 Å [III] resulting in a rather small value for the Coulombic term (0.04 eV in benzonitrile). For the triad compounds [1] r_{DA} is longer decreasing the extend of the Coulombic term further. Thus, the energies of the CS states were calculated from the differences between the two potentials ignoring the Coulombic interactions for all the compounds in this study.

3.5 Photovoltage and photocurrent

To see how the studied molecules might function in solar cell applications photovoltage and photocurrent generation of the solid thin film samples of porphyrin-porphyrin-fullerene triad SAMs on semitransparent ITO electrodes were tested [II].

Time-resolved photovoltage measurements were carried out using the time-resolved Maxwell displacement charge technique [75]. Prior to the photovoltage measurements 20 Langmuir-Blodgett monolayers of octadecylamine (ODA) were deposited on top of the samples to insulate the active layers from the InGa electrode [76,77]. The ITO layer of the samples was used as the

top electrode and a drop of liquid InGa alloy was applied as the bottom electrode. Excitation was carried out with 10 ns laser pulses at 436 nm arriving to the active layers through the transparent ITO. The time profile of the photovoltage signal after the excitation was recorded with an oscilloscope.

The photocurrent measurements were carried out with a system consisting of a voltammetric analyzer and a three-electrode cell with the ITO layer as the active electrode (area 0.07 cm^2), platinum wire counter electrode, and Ag/AgCl (sat. KCl) reference electrode. The photocurrent was induced by a step-wise excitation from a xenon lamp coupled with a monochromator. The light intensity was monitored with an optical power meter and corrected. Both anodic and cathodic photocurrent generation in the samples was examined using aqueous electrolyte solutions of 5 mM 1,1-dihexyl-4,4'-dipyridinium diperchlorate (HV^{2+}) and 50 mM triethanol amine (TEA), respectively. HV^{2+} supports the rational direction of the electron movement from porphyrin to C_{60} in the studied triad samples, *i.e.* acts as an electron acceptor, while TEA as an electron donor acts better with the opposite direction of the electron flow. Na_2SO_4 (0.1 M) was used as the supporting electrolyte in all the measurements and the electrolyte solutions of HV^{2+} and TEA were saturated by oxygen or by nitrogen, respectively.

4 Results and discussion

4.1 Porphyrin-porphyrin-fullerene triads

Three triad structures were studied to determine the role of the side porphyrin as a secondary electron donor to the previously studied porphyrin-fullerene dyad [19]. In addition to fundamental studies of the triad compounds in solutions [I], photovoltaic behaviour of the structures was tested in thin solid films [II]. This section summarizes the results of the triad studies both in solutions and in films.

4.1.1 Electron transfer in solutions

4.1.1.1 Effect of the second porphyrin unit

The steady state absorption spectra of all the triads indicated some interactions between the porphyrin-fullerene dyad unit P_1C and side porphyrin P_2. The spectra of the triads were approximately superpositions of the spectra of the dyad reference **P_1C** and the porphyrin reference (see paper I for the molecular structures), but for example the Soret band was weaker and slightly shifted to the red. The emission spectra of the triads showed that the porphyrin-fullerene moiety P_1C preserves its exciplex nature as it was observed for the corresponding dyad compounds [19]. However, the emission of the exciplex, observed around 700-950 nm in non-

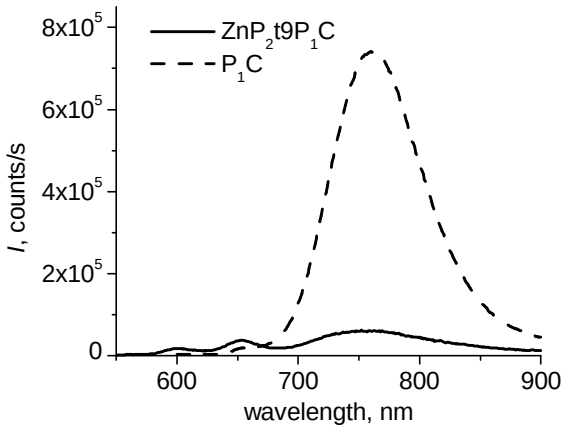

Figure 4.1. Emission spectra of **ZnP_2t9P_1C** and **P_1C** in toluene with the same absorbance at the excitation wavelength 428 nm.

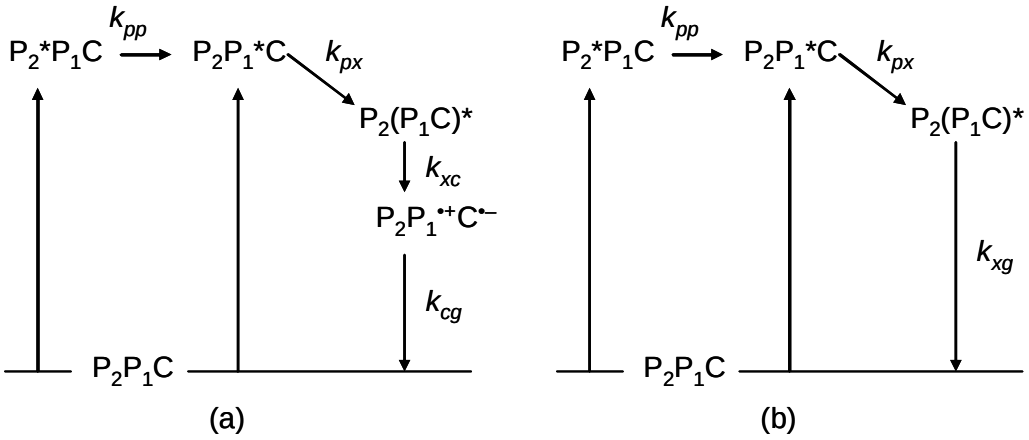

Figure 4.2. Reaction schemes for triads **P_2c10P_1C** and **P_2t9P_1C** (a) in benzonitrile and (b) in toluene. Internal conversion from the second excited singlet state of porphyrin (where the excitation in these measurements promotes the molecule) to the first excited singlet state has been omitted for clarity.

polar solvent, was weaker in the triads compared to the dyad **P_1C** (Figure 4.1) indicating that the exciplex transforms into another transient, *i.e.* to a CS state, more efficiently in the triads.

The transient absorption measurements with the pump-probe method revealed that attaching a free-base porphyrin as the second porphyrin unit to the free-base porphyrin-fullerene dyad (triads **P_2c10P_1C**, see paper I for the molecular structure, and **P_2t9P_1C**, Figure 3.1) changes the photophysical behaviour of the dyad very little. Formation of a CS state between the inner porphyrin unit, P_1, and fullerene via the exciplex $(P_1C)^*$ was observed in benzonitrile. This is essentially the same scheme as for the corresponding dyad [19]. However, the scheme (Figure 4.2a) must be extended with the energy transfer from the outer porphyrin unit, P_2, to the inner one, if the outer porphyrin is the one initially excited. As in the dyad studied earlier [19], the CS state is not detected in triads **P_2c10P_1C** and **P_2t9P_1C** in non-polar toluene, but the exciplex is seen to relax directly to the ground state (Figure 4.2b). Rate constant for the slow relaxation of the exciplex (k_{xg}) in toluene was determined with TCSPC (Table 4.1). However, it is possible (and likely, as has been discussed for the corresponding dyad [19]) that the CS state is formed also in toluene, but it is invisible in the time-resolved measurements because it decays much faster than it is formed.

The rate constants for the exciplex formation (k_{px}) and relaxation (k_{xg}) are approximately the same for triads **P_2c10P_1C** and **P_2t9P_1C** in toluene as for the corresponding dyad (Table 4.1). Also in benzonitrile the exciplex and the CS state are formed with equal rates (k_{px} and k_{xc}, respectively) as in the dyad **P_1C**, but the CS state $P_2P_1^{\bullet+}C^{\bullet-}$ in the triads lasts over two times

Table 4.1. Rate constants (10^9 s^{-1}) for the triads **P_2c10P_1C** and **P_2t9P_1C** and the reference dyad **P_1C** [19].

compound	solvent	k_{pp}	k_{px}	k_{xg}	k_{xc}	k_{cg}
P_1C	benzonitrile		10000		100	2.6
	toluene		6000	0.34		
P_2c10P_1C	benzonitrile	~100	7000[a]		~100	1.1
	toluene	59[a] / 4[a]	5000[a]	0.38		
P_2t9P_1C	benzonitrile	27[a] / 2.2[a]	6700[a]		~100	1.1
	toluene	26	5000	0.36		

[a] From the up-conversion measurements.

longer (rate constant k_{cg}). The reason for this could be that the attached P_2 prevents the solvent molecules from approaching $P_1^{\bullet+}$, *i.e.* the cation is shielded by the outer porphyrin.

As opposed to a free-base porphyrin, a Zn porphyrin attached to the free-base porphyrin-fullerene dyad (triad **ZnP_2t9P_1C**) alters the photophysics of the dyad dramatically. The pump-probe measurements were carried out with two different excitation wavelengths: at 515 nm free-base porphyrin is excited in roughly 80 % of the molecules and at 555 nm Zn porphyrin is excited in 70 % of the molecules. The results obtained at the two different wavelengths are very similar to each other showing that extremely rapid ET to yield the final CS state $ZnP_2^{\bullet+}P_1C^{\bullet-}$ occurs independent of the excited porphyrin unit.

Because of the extremely rapid electron transfer yielding the CS state, the intermediates of the reaction can't be resolved with the instrument. Still, the reaction is evidently multi-step. Based on both steady-state and time-resolved measurements the same scheme (Figure 4.3) can be suggested in both benzonitrile and toluene. Exciplex emission was clearly seen for **ZnP_2t9P_1C** (Figure 4.1) and it is reasonable to conclude that ET occurs via the exciplex, if the free-base porphyrin P_1 is excited. However, it is most probable that the exciplex is not formed, if the Zn porphyrin unit of the triad is excited. In order for the exciplex to be formed, energy transfer from ZnP_2 to P_1 should first take place. Measurements done on porphyrin dimer **ZnP_2P$_1$** (see paper I for the molecular structure) show that energy transfer from ZnP_2 to P_1 occurs rather slowly (in 80 ps). In the triad the CS state is formed in less than 0.2 ps even when Zn porphyrin is excited and the reaction can't occur via the energy transfer and exciplex formation.

Nevertheless, evidence of an intermediate state preceding the final CS state was obtained in the pump-probe measurements in toluene also when the Zn porphyrin moiety of the triad was

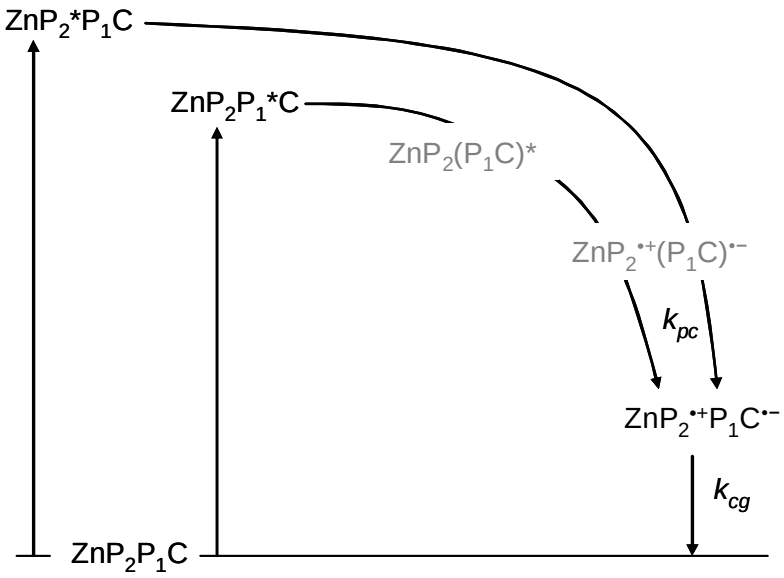

Figure 4.3. Reaction scheme for triad **ZnP$_2$t9P$_1$C**. (k_{pc} is the rate constant for the transitions from the locally excited states of P_2 or P_1 to the final CS state $ZnP_2^{\bullet+}P_1C^{\bullet-}$. The two intermediates given in grey colour were not well identified in the measurements; see the text for discussion.)

excited. The spectral similarity of this intermediate with that of the final CS state indicates, that also the intermediate is a CS state. The results show, that Zn porphyrin is involved in this state, *i.e.* the positive charge is on ZnP_2. The negative charge could be on the free-base porphyrin P_1, but measurements of the dimer **ZnP$_2$P$_1$** showed that such state is not formed. Therefore, the most likely explanation for the intermediate is a state, where the electron is delocalized around the inner porphyrin and fullerene $ZnP_2^{\bullet+}(P_1C)^{\bullet-}$. Such a state is reasonable as an intermediate also between the exciplex and the final CS state in triad **ZnP$_2$t9P$_1$C**. Both the suggested intermediate CS state and the exciplex indicate that the inner porphyrin and fullerene act as a single moiety P_1C in the triad **ZnP$_2$t9P$_1$C**. This is reasonable taking into account the ground state and excited state interaction of the corresponding porphyrin-fullerene dyad [19] observed as visible changes in the absorption and emission properties compared to the individual chromophores.

Rate constant for the formation of the final CS state from the excited state of either ZnP_2 or P_1, k_{pc}, is 10×10^{12} s^{-1} in both toluene and in benzonitrile, which is about a 100 times faster than the formation of the CS state in the reference dyad **P$_1$C** (Table 4.1). The BET reaction occurs with a rate constant $k_{cg} = 1.8 \times 10^9$ s^{-1} in toluene and $k_{cg} = 6.6 \times 10^9$ s^{-1} in benzonitrile. Thus, also BET is faster in the triad **ZnP$_2$t9P$_1$C** compared to dyad **P$_1$C**. This seems contradictory based on the distance dependence of the ET rate discussed in section 2.1. However, it should be taken into account that the CS state in **ZnP$_2$t9P$_1$C** has a lower energy than that in **P$_1$C**, which

should lead to a shorter lifetime in the Marcus inverted region. Actually, the CS state lifetime of the triad is still a few times longer than that of the **ZnP$_1$C** dyad (k_{cg} = 16 × 10^9 s^{-1} in benzonitrile [19]), which is otherwise the same as dyad **P$_1$C**, but contains Zn as the centre atom of porphyrin, and is expected to have similar CS state energetics to the triad. Consequently, increase in the charge separation distance results in increase of the CS state lifetime, indeed. A longer lifetime of the CS state is observed for the triad in toluene, which also is expected based on the Marcus theory for BET occurring in the inverted region.

4.1.1.2 Effect of the central metal on the second porphyrin unit

As discussed in the previous section, the central metal on the second porphyrin unit attached to the free-base porphyrin-fullerene dyad has a major effect on the behaviour of the compound. The DPV measurements show, that there is practically no driving force for a reaction $P_2P_1^{\bullet+}C^{\bullet-} \rightarrow P_2^{\bullet+}P_1C^{\bullet-}$ in triad **P$_2$t9P$_1$C**, because the two porphyrin units have very similar oxidation potentials. Instead, the Zn porphyrin unit in Zn derivative of **P$_2$t9P$_1$C**, triad **ZnP$_2$t9P$_1$C**, has a lower oxidation potential than the free-base porphyrin resulting in a clearly exergonic reaction $ZnP_2P_1^{\bullet+}C^{\bullet-} \rightarrow ZnP_2^{\bullet+}P_1C^{\bullet-}$ with $-\Delta G$ = 0.3 eV. Thus, it is not surprising that the final CS state was not observed in the transient absorption measurements of **P$_2$t9P$_1$C**, but was formed extremely rapidly in **ZnP$_2$t9P$_1$C**.

4.1.1.3 Effect of distance and orientation between the two porphyrin units

The two triads **P$_2$c10P$_1$C** and **P$_2$t9P$_1$C** can be compared to evaluate the effect of the distance and mutual orientation of the two porphyrin units. **P$_2$c10P$_1$C** is a *cis* structure with the linkers on the adjacent phenyl groups of the outer porphyrin P$_2$ and **P$_2$t9P$_1$C** is a *trans* structure with the linkers on the opposite phenyl groups. In addition, the linkers of **P$_2$c10P$_1$C** are one bond longer than the ones of **P$_2$t9P$_1$C**. The centre-to-centre distance of P$_2$ and P$_1$ can be roughly estimated as 13 Å and 9 Å for **P$_2$c10P$_1$C** and **P$_2$t9P$_1$C**, respectively. The somewhat shorter linker lengths and especially the more compact sandwich-like structure, achieved with the *trans* positions of the linkers in **P$_2$t9P$_1$C**, result in a more efficient energy transfer from P$_2$ to P$_1$ indicated by roughly 2.5 times stronger quenching of the porphyrin monomer emission around 650 nm and 720 nm.

Because of the efficient energy transfer from P$_2$ to P$_1$, also the exciplex formation is more efficient in the *trans* structure **P$_2$t9P$_1$C**. The DAS measured with TCSPC for **P$_2$c10P$_1$C** and **P$_2$t9P$_1$C** show two simultaneous processes: energy transfer from P$_2$ to P$_1$ and formation of the exciplex. The component corresponding to the exciplex emission is more than two times higher

in intensity for **P_2t9P_1C** than for **P_2c10P_1C** relative to the component representing the porphyrin monomer emission (see discussion and Figure 9 in paper I).

The energy transfer rates (k_{pp}) for **P_2c10P_1C** and **P_2t9P_1C** are given in Table 4.1. The up-conversion measurements showed that the energy transfer is bi-exponential, *i.e.* two decay components were obtained for the emission of P_2. This makes the comparison of energy transfer rates of the two triads difficult. It should also be taken into account that the energy transfer rates of Table 4.1 are obtained from two different measurements, up-conversion and pump-probe. The rates from up-conversion are more accurate, but for some of the samples reliable results were not obtained from these measurements, because of degradation of the samples by the intense laser excitation. Thus rates from the pump-probe results are given as indicated in the Table.

4.1.2 Electron transfer in films

4.1.2.1 Film structures

As described in section 3.1 the triad film structures were prepared as successive self-assembled monolayers of Zn porphyrin and free-base porphyrin-fullerene dyad. Due to the preparation method, it is possible that the dyad molecules did not attach precisely on each underlying Zn porphyrin, but can cover more than one Zn porphyrin. In fact, several measurements proved that this is the case for the studied samples. Even though in reality there is more than one Zn porphyrin per each dyad in the film, the structures are denoted as "triads" for convenience.

First evidence of the extremely tightly packed Zn porphyrin SAMs is the very high absorbance of the reference samples ***cis*-ZnP** and ***trans*-ZnP**. An average area per molecule (mean molecular area, mma) can be estimed from the absorbance as

$$mma = \frac{\varepsilon}{N_A A}, \tag{10}$$

where ε is the molar absorptivity, N_A is the Avogadro constant and A is the absorbance of the layer. The calculated mma values (0.54 nm^2 and 0.78 nm^2 for ***cis*-** and ***trans*-ZnP**, respectively) are considerably smaller than what can be expected for a porphyrin monolayer with porphyrin rings ordered parallel to the substrate surface. For comparison, mma values of 3.7 nm^2 and 2.3 nm^2 have been reported for a corresponding free-base porphyrin SAM with four linkers attached to the ITO surface [48] and for a similar Langmuir-Blodgett monolayer [78], respectively. Thus,

it is clear that neither ***cis*-** nor ***trans*-ZnP** macrocycles are parallel to the substrate surface. For ***cis*-ZnP** the area per molecule is so small that it is more likely that the layer is not a monolayer at all, but the molecules are somehow imbricated on top of each other. This is possible taking into account the relatively long and flexible linkers that connect the compound to the surface.

The absorption spectra of the ***cis*-** and ***trans*-ZnP** samples on ITO show also broader and red-shifted Soret band compared to the reference Zn porphyrin sample measured in toluene solution, indicating aggregation of Zn porphyrins, which is characteristic for densely packed layers [79]. Aggregation in the dense Zn porphyrin layers is confirmed also by the self-quenching observed in the porphyrin emission around 650 nm compared to Zn porphyrin reference in solution.

A layer of double-bridged free-base porphyrin-fullerene dyad was assembled on top of the ***cis*-** and ***trans*-ZnP** layers to obtain ***cis*-triad** and ***trans*-triad** samples, respectively (see paper II for the sample preparation scheme). It was found out, that attaching the dyad on top of the Zn porphyrin layer increases the absorption of the samples only slightly indicating that the layer is not densely packed. For ***trans*-triad** it was not evident from the absorption spectrum that the dyad layer had been attached on the Zn porphyrin layer at all. However, the emission spectrum of the ***trans*-triad** sample showed characteristic exciplex emission confirming the dyad attachment. Considering the earlier studies of the corresponding dyad SAM [48], where only very small differences in the absorption spectra were observed between the SAM sample and the reference in solution, it can be expected that the dyad units in the triad samples are aligned parallel to the substrate.

4.1.2.2 Photocurrent and photovoltage of the films

The photocurrent measurements carried out for the triad films on ITO in the presence of HV^{2+} and TEA show similar shapes of the current-voltage (IV) curves (Figure 4.4) indicating electron transfer in the direction determined by the sample structure: ITO $\rightarrow$ Zn porphyrin $\rightarrow$ free-base porphyrin $\rightarrow$ fullerene $\rightarrow$ electrolyte. The highest photocurrents were obtained in the presence of HV^{2+} as expected.

The shapes of the curves for the triad samples (Figure 4.4) are comparable to the ideal IV-curve. Internal quantum efficiencies of the photocurrent generation, ϕ, are given in Table 4.2. The quantum efficiencies of the triad samples can be compared to values obtained for the corresponding porphyrin-fullerene dyad SAM sample studied previously [48]. For the dyad a higher value was obtained in the presence of TEA than in HV^{2+}, which is surprising taking into account that TEA supports the opposite direction of electron movement than the sample structure. More reasonably, the highest ϕ for ***cis*-triad** and ***trans*-triad** were calculated from the

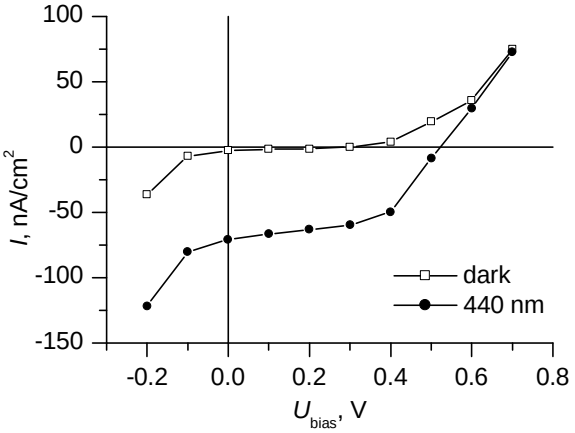

Figure 4.4. IV-curves of ***cis*-triad** sample on ITO in the presence of HV^{2+}.

measurements in the presence of HV^{2+} and these are 2 and 3 times higher compared to the dyad, respectively. The ϕ value of the ***trans*-triad** in the presence of HV^{2+} is roughly two times higher than that of the ***cis*-triad**. This is expected on the grounds of the measurements of the triads in solution [I]: more efficient interaction occurs between the two porphyrin moieties in the *trans*-structure than in the *cis*-structure.

In addition to the IV-curves, the action spectra were recorded for the samples in the photoelectrochemical cell. The action spectra follow the absorption of the sample films on the ITO quite closely for all the samples. Especially the Q-band shapes of the absorption and action spectra match each other for the triad samples, proving that both Zn and free-base porphyrins act as the photoactive sensitizers of these samples.

Strong photovoltage signals were detected for both ***cis*-triad** and ***trans*-triad** on ITO even with very low excitation light intensities. The direction of the electron movement is as expected from ITO to SAM for both triad structures. Photovoltage reached with the ***cis*-triad** sample was approximately 4 times higher in amplitude compared to the ***trans*-triad**. This seems to be in contradiction with the results of the photocurrent measurements, where the higher

Table 4.2. Quantum efficiencies of photocurrent generation. See paper II for the description on how the quantum efficiencies were calculated.

	ϕ /%	
sample	**HV^{2+}**	**TEA**
***cis*-triad**	0.62	0.16
***trans*-triad**	1.25	0.98
dyad [48]	0.36	2.1

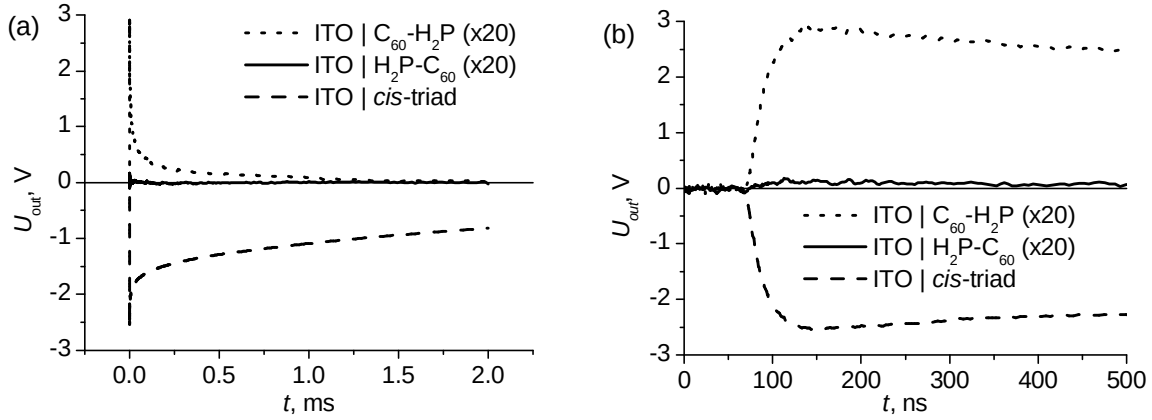

Figure 4.5. Photovoltage responses of ***cis*-triad** and corresponding $H_2P–C_{60}$ and $C_{60}–H_2P$ dyad SAMs on ITO plotted in two different time scales with 0.1 mJ/cm^2 excitation energy density at 436 nm. Amplitudes of the dyad samples have been multiplied for comparison as indicated in the figure.

quantum efficiencies were obtained for ***trans*-triad**, but can be explained on the grounds of the different measuring principles of the two methods: in photovoltage measurements interaction between the ITO electrode and the compound is not necessary, but in the photocurrent measurements the electrons need to flow from ITO to the electrolyte. Thus, the closer contact of Zn porphyrins of ***trans*-triad** with the ITO surface allows more efficient interaction and photocurrent generation. Instead, the higher absorption and slightly longer CS distance of ***cis*-triad** result in the exceptionally strong photovoltage response.

Comparing the photovoltage response of the ***cis*-triad** sample and the corresponding ITO | $H_2P–C_{60}$ and ITO | $C_{60}–H_2P$ dyad SAM samples studied earlier [48] one can see (Figure 4.5) that the densely packed Zn porphyrin layer has a huge effect on the behaviour of the sample. The dyad sample with structure ITO | $H_2P–C_{60}$, which is directly comparable with the ***cis*-triad** sample (oriented in the same direction but without the Zn porphyrin layer), gives a very weak positive signal indicating that the electrons are moving in the opposite direction than expected, but a strong negative signal is seen for the triad. Ignoring the fact that the dyad sample acts in the 'wrong' direction and just comparing the absolute value of the maximum voltage obtained, the ***cis*-triad** sample gives 280 times higher voltage response. For sure the triad sample also absorbs more efficiently because of the very dense layer of Zn porphyrins, but actually absorption at the excitation wavelength is only 12 times higher for the triad.

The reverse oriented dyad sample, ITO | $C_{60}–H_2P$, shows a signal corresponding to ET in the expected direction taking its orientation into account, and also the signal amplitude is better comparable to the signal of the ***cis*-triad** sample: the absolute value of the maximum voltage is

17 times higher and absorption 6 times higher for the triad. Still, the difference in absorption cannot completely explain that in the photovoltage response. Instead, the enhanced operation of the triad is quite reasonable taking into account the approximately three times longer CS distance achieved in the triad due to the secondary electron donor. The longer CS distance results also in considerably longer living photovoltage signal in the triad sample as can be seen in Figure 4.5a.

4.2 Phthalocyanine-fullerene dyads

Altogether six different double-linked phthalocyanine-fullerene dyads were studied to determine a common scheme for the photoinduced electron transfer. Similar behaviour, e.g. exciplex mediated ET, as determined in previous studies on comparable phytochlorin- and porphyrin-fullerene dyads [12,14,15,19,51-53], was expected also for the phthalocyanine-fullerene compounds. This section summarizes the results obtained for the phthalocyanine-fullerene dyads and comparison with the previously studied phytochlorin- and porphyrin-fullerene dyads is done in section 4.3.

The reaction scheme determined for photoinduced ET of the studied phthalocyanine-fullerene dyads is given in Figure 4.6. Depending on the excitation wavelength the phthalocyanine chromophore of the dyad is promoted to the second, $^{2S}Pc^*{-}C_{60}$, or the first excited singlet state, $^{1S}Pc^*{-}C_{60}$. Internal conversion from $^{2S}Pc^*{-}C_{60}$ to $^{1S}Pc^*{-}C_{60}$ is too fast to be resolved accurately with the instruments used in this study and this transition is drawn as a dotted arrow in Figure 4.6. As will be discussed in section 4.2.1 $^{1S}Pc^*{-}C_{60}$ is in equilibrium with the exciplex, $(Pc{-}C_{60})^*$. Formation of the CS state, $Pc^{\bullet+}{-}C_{60}^{\bullet-}$, follows from $(Pc{-}C_{60})^*$ and BET occurs directly to the ground state. In general, this scheme is the same as the ones reported

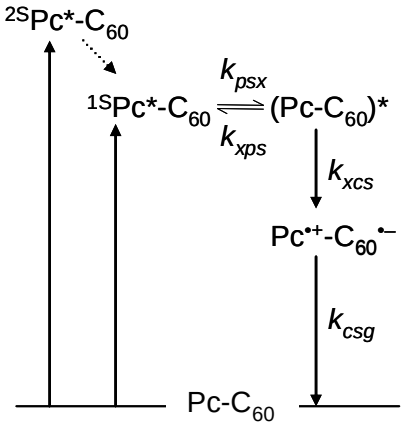

Figure 4.6. Reaction scheme for photoinduced electron transfer in phthalocyanine-fullerene dyads. See text for explanations.

earlier for the comparable phytochlorin- and porphyrin-fullerene dyads [12,14,15,51-53]. Exceptions to the general scheme of Figure 4.6 are discussed in sections 4.2.2 and 4.2.3.

4.2.1 Exciplex intermediate in ET

The steady state emission studies of the phthalocyanine-fullerene dyads give somewhat unexpected results: the characteristic exciplex emission clearly seen in non-polar solvent for the comparable porphyrin-fullerene compounds (see Figure 4.1 for porphyrin-fullerene dyad and triad emission) is very weak for the phthalocyanine-fullerene dyads (**ZnPc-C_{60}tb** as an example in Figure 4.7). Quenching of the phthalocyanine singlet state emission indicates an efficient reaction with the fullerene moiety of the dyad. Based on the shape of the emission spectra and the solvent dependence of the quenching (more efficient in polar solvent for all studied dyads) it can be concluded, that rapid electron transfer from the phthalocyanine singlet excited state to fullerene is behind the quenching. However, the possibility of exciplex formation exists regardless of the weak evidence in the emission spectrum, because also the exciplex emission may be quenched by rapid ET (as it was for porphyrin-porphyrin-fullerene triads discussed in section 4.1.1) or it can overlap the phthalocyanine emission. Quenching via ET is the more likely reason, because it can be estimated that the maximum of the exciplex emission should be seen at approximately 800 nm (see paper IV for more detailed discussion), *i.e.* the exciplex emission should be well-separated from the phthalocyanine singlet excited state emission.

The alternative process of energy transfer to fullerene can be ruled out, because the quenching of phthalocyanine emission is not accompanied by appearance of fullerene emission around 700-800 nm [V]. In principle, the energy transfer could precede ET and not seeing emission from

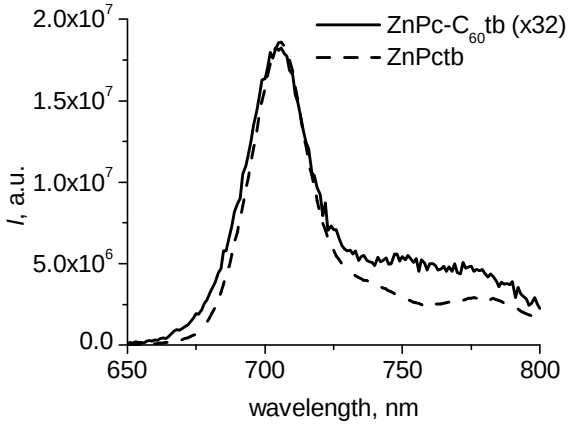

Figure 4.7. Fluorescence spectra of **ZnPc-C_{60}tb** and **ZnPctb** in toluene excited at 625 nm. The spectrum of the dyad has been multiplied for comparison as indicated in the figure.

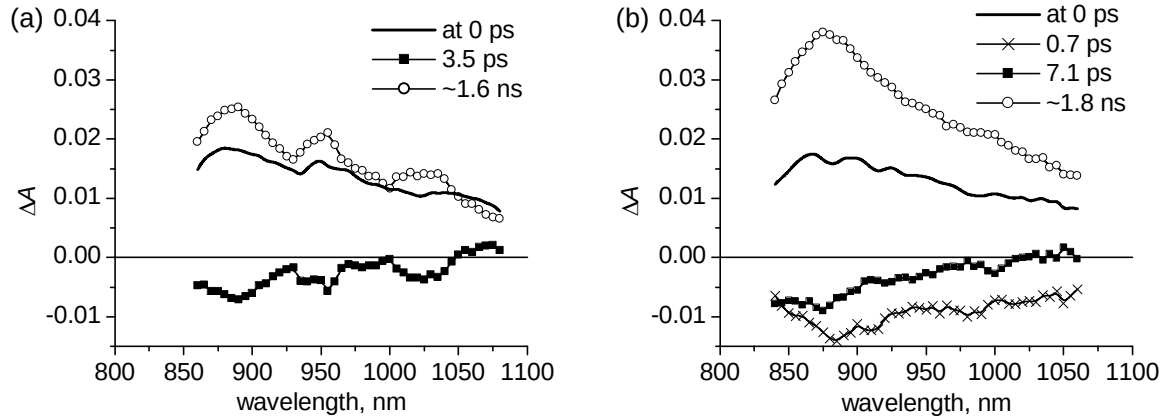

Figure 4.8. Decay component spectra and calculated time-resolved absorption spectra at 0 delay time for toluene solutions of (a) **H_2PcF-1** [III] and (b) **H_2Pc-C_{60}tb** [IV].

$Pc^{-}{}^{1S}C_{60}$* could be because of quenching of $^{1S}C_{60}$* by ET like discussed for the exciplex above. However, this can be excluded, because the time-resolved absorption measurements did not show any recovery of the bleaching of the phthalocyanine Q band before the very end of the photoinduced reaction, indicating that the phthalocyanine moiety of the dyad does not return to its ground state until after BET from the CS state [80]. Furthermore, the flash-photolysis measurements revealed that ET does not occur from $Pc^{-}{}^{1S}C_{60}$* (see section 4.2.3).

The first set of phthalocyanine-fullerene dyads [III] studied for the Thesis exhibited limited solubility in non-polar solvents making it difficult to further investigate the existence of the exciplex intermediate. The pump-probe measurements of these dyads show only two transient states: the phthalocyanine first excited singlet state and the CS state (dyad **H_2PcF-1** as an example in Figure 4.8a). Figure 4.8a presents the decay component spectra (see section 3.3.1) obtained from the global fit of differential absorption decay curves and the calculated spectrum at 0 delay time, *i.e.* directly after excitation. The spectrum at 0 delay time represents the first excited singlet state of phthalocyanine, which has somewhat stronger absorbance compared to the ground state (increase in ΔA) at this wavelength range. The first component of the fit (3.5 ps time constant) shows negative amplitude, *i.e.* the corresponding transition results in increase of absorbance at these wavelengths. The transition can be attributed to the formation of the CS state from the increasing absorbance at the characteristic wavelengths of phthalocyanine cation and fullerene anion. The phthalocyanine cation band appears at slightly different wavelength depending on the metal substitution: around 900 nm or 850 nm for free-base and Zn compounds, respectively [68]. The double-linked fullerene anion shows a broad absorption band around 900-

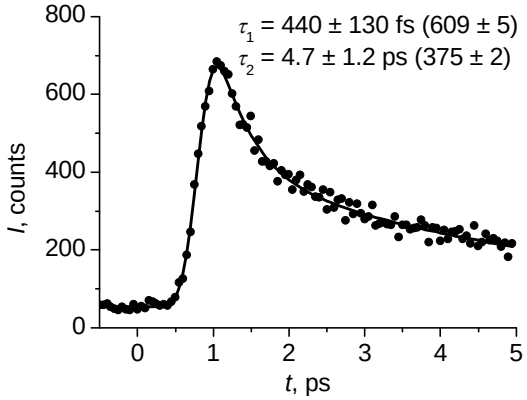

Figure 4.9. Fluorescence decay of **ZnPc-C_{60}tb** in benzonitrile excited at 420 nm and monitored at 710 nm. The lifetimes, τ_i, and amplitudes (in parentheses) of the bi-exponential fitting are given in the figure.

1100 nm [19] as opposed to the well-defined band at 1060 nm for pristine C_{60} [81]. The second decay component (~1.6 ns time constant) is the relaxation of the CS state to the ground state and since the CS state is the last transient of the reaction, the decay component spectrum (~1.6 ns) is also the differential absorption spectrum of the CS state.

Solubility of the dyad **H_2PcF-1** was improved by changing the ethyl ester end groups of the linkers to *tert*-butyl esters in dyad **H_2Pc-C_{60}tb**. The better solubility allowed pump-probe measurements with a higher concentration resulting in better accuracy of the data. As can be seen in Figure 4.8, the signal amplitude is higher and the signal-to-noise ratio better for the more concentrated solution of **H_2Pc-C_{60}tb**. The spectrum calculated at 0 delay time and the final component seen, are clearly the same for both **H_2PcF-1** and **H_2Pc-C_{60}tb**, *i.e.* the first excited singlet state of phthalocyanine and the CS state, respectively. However, due to the improved accuracy, a third component was resolved in the fitting of pump-probe data for **H_2Pc-C_{60}tb** revealing that there is an intermediate state in the ET reaction. On grounds of the spectral similarity of the resolved intermediate and the CS state (see paper IV), and the earlier studies of phytochlorin- and porphyrin-fullerene dyads [12,15,19,51-53], the intermediate can be assigned as the exciplex.

The up-conversion measurements of all the studied phthalocyanine-fullerene dyads [III,IV] gave a consistent result: the decay of the first excited singlet state of phthalocyanine is bi-exponential for these compounds (see **ZnPc-C_{60}tb** in benzonitrile as an example in Figure 4.9). This indicates that the monitored state, the phthalocyanine singlet state, is in equilibrium with the following state, *i.e.* the exciplex. The rate constants of the equilibrium, k_{psx}, k_{xps} and k_{xcs} (Figure

4.6, Table 4.3), can be calculated from the experimental lifetimes (τ_1, τ_2) and amplitudes (a_1, a_2) as [14,80]

$$\begin{aligned} k_{psx} &= \frac{s\beta_1 + \beta_2}{-s-1} \\ k_{xcs} &= \beta_1\beta_2 k_{psx}^{-1} \\ k_{xps} &= -\beta_1 - \beta_2 - k_{psx} - k_{xcs} \end{aligned} \tag{11}$$

where $s = a_1/a_2$, $\beta_1 = -1/\tau_1$ and $\beta_2 = -1/\tau_2$. Furthermore, knowing the rate constants of the equilibrium, it is possible to estimate the energy difference of the two states in equilibrium as

$$\Delta E_{psx} = k_B T \ln\left(\frac{k_{psx}}{k_{xps}}\right), \tag{12}$$

and from this the exciplex state energy, E_x, can be determined (Table 4.3).

Table 4.3. Rate constants (see Figure 4.6) and state energies of the ET reaction. E_{ps}, E_x, and E_{cs} are the state energies of the phthalocyanine first excited singlet state, the exciplex, and the CS state, respectively.

compound	**solvent**	E_{ps} /eV	k_{psx} / k_{xps} /10^9 s^{-1}	E_x /eV	k_{xcs} /10^9 s^{-1}	E_{cs} /eV	k_{csg} /10^9 s^{-1}
H_2PcF-1	toluene	1.72	-[a]	-[a]	-[a]	-[b]	0.1-0.8[c]
	benzonitrile	1.70	900 / 320	1.67	110	1.22	12
H_2PcF-2	toluene	1.67	-[d]	-[d]	-[d]	-[b]	<0.8[c]
	benzonitrile	1.65	-[d]	-[d]	-[d]	1.22	19
ZnPcF	toluene	1.77	59 / 42	1.75	19	-[b]	<0.8[c]
	benzonitrile	1.77	130 / 32	1.75	64	1.16	18
H_2Pc-C_{60}tb	toluene	1.72	2110 / 1350	1.71	280	-[b]	0.1-0.8[c]
	benzonitrile	1.70	1800 / 620	1.67	290	1.24	14
ZnPc-C_{60}tb	toluene	1.77	960 / 620	1.76	190	-[b]	0.8
	benzonitrile	1.77	1620 / 770	1.75	310	1.16	33

[a] Could not be determined because of poor solubility of the compound in toluene.

[b] DPV could not be carried out in non-polar toluene.

[c] Could not be determined accurately, because the process falls in the time gap of the two transient absorption measurement systems used in this study.

[d] Up-conversion could not be carried out because emission of the compound is too close to the laser fundamental harmonic of the instrument.

4.2.2 Effect of central metal substitution

The effect of changing the central metal on the phthalocyanine moiety of the dyad was studied with a series of three dyads with otherwise the same structure: **H_2Pc-C_{60}tb**, **ZnPc-C_{60}tb** and **CuPc-C_{60}tb** (Figure 3.1). The photoinduced behaviour of **H_2Pc-C_{60}tb** and **ZnPc-C_{60}tb** [IV] is very similar and was described in the previous section. The energy of the CS state is slightly lower for **ZnPc-C_{60}tb** than for **H_2Pc-C_{60}tb**, which increases the driving force of ET for the former. However, the exciplex mediated ET is rapid in both **H_2Pc-C_{60}tb** and **ZnPc-C_{60}tb** (see Table 4.3). The rate constants for the equilibrium between ^{1S}Pc*−C_{60} and (Pc−C_{60})* and for ET from (Pc−C_{60})* are very similar for the two dyads in benzonitrile and in toluene actually somewhat faster reactions occur in **H_2Pc-C_{60}tb** than in **ZnPc-C_{60}tb**. BET is approximately two times faster for **ZnPc-C_{60}tb** (with $-\Delta G_{BET}$ = 1.16 eV) than for **H_2Pc-C_{60}tb** (with $-\Delta G_{BET}$ = 1.24 eV), which is consistent with BET occurring in the inverted region [58].

The dyad with copper as the central metal, **CuPc-C_{60}tb**, acts completely differently than **H_2Pc-C_{60}tb** and **ZnPc-C_{60}tb**. The energy of the CS state in benzonitrile was estimated with DPV to be 1.19 eV, *i.e.* lower than for **H_2Pc-C_{60}tb** and higher than for **ZnPc-C_{60}tb**, but ET does not occur in **CuPc-C_{60}tb**. The very different behaviour of Zn and Cu phthalocyanine-fullerene dyads can be explained by the different character of the central metal ions: the electron configuration of Cu^{2+} includes an unpaired electron making the metal centre paramagnetic while for Zn^{2+} all the electrons are paired. The unpaired electron of Cu^{2+} couples with the π electron system of the phthalocyanine in the dyad resulting in quite rapid intersystem crossing from the phthalocyanine singlet state to the triplet [68,82]. The intersystem crossing is so rapid that it prevents ET in **CuPc-C_{60}tb**. The pump-probe results (Figure 4.10) show no increase in absorbance in the 850-

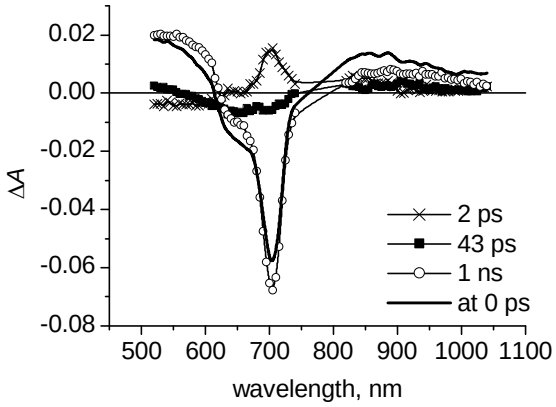

Figure 4.10. Decay component spectra and calculated time-resolved absorption spectrum at 0 delay time for benzonitrile solution of **CuPc-C_{60}tb** excited at 390 nm.

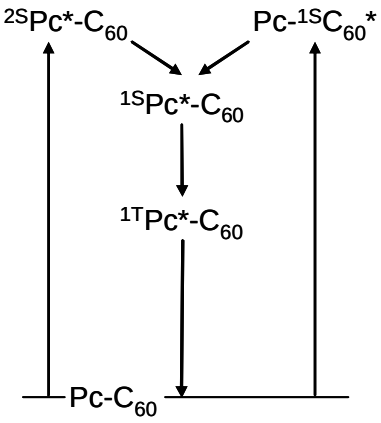

Figure 4.11. Reaction scheme for photoinduced reactions of **CuPc-C_{60}tb**.

1100 wavelength range, where the phthalocyanine cation and the fullerene anion absorb. Instead the final component (1 ns time constant) shows somewhat higher absorbance around 500-600 nm characteristic for the triplet state of phthalocyanine (see further discussion in the following section). Thus it seems that excitation of the Cu phthalocyanine in the dyad **CuPc-C_{60}tb** results in intersystem crossing $^{1S}Pc^*-C_{60} \rightarrow {}^{1T}Pc^*-C_{60}$ (Figure 4.11). The tri-exponential fitting can be explained taking into account that at the excitation wavelength of the measurement fullerene absorbs almost as much as phthalocyanine. Thus energy transfer $Pc-{}^{1S}C_{60}^* \rightarrow {}^{1S}Pc^*-C_{60}$ accounts for the first component of the fit (Figure 4.11).

4.2.3 Triplet state interactions

As was mentioned in the previous section, phthalocyanine triplet state is formed efficiently in **CuPc-C_{60}tb** (Figure 4.11). The pump-probe measurements give a lifetime of roughly 1 ns for the Cu phthalocyanine triplet excited state, which is very short for a triplet state in general, but can be explained by the paramagnetic nature of the Cu central metal resulting in efficient intersystem crossing reactions as was discussed above. The flash-photolysis measurements of **CuPc-C_{60}tb** confirmed that the triplet state is the final state of the reaction and ET does not take place in this dyad. Such behaviour, where intersystem crossing dominates over ET, is certainly an exception in this series of phthalocyanine-fullerene dyads, but transitions to triplet states were found to occur also in reactions of **H_2Pc-C_{60}tb** and **ZnPc-C_{60}tb**.

The general scheme for ET in the phthalocyanine-fullerene dyads (Figure 4.6) is sufficient in benzonitrile, but it needs minor modification in non-polar toluene (Figure 4.12). The flash-photolysis studies show that the triplet state of phthalocyanine is formed from the CS state in roughly 20 % of the dyad molecules in toluene. Direct relaxation to the ground state is still the major path for the decay of the CS state, but since this BET reaction is pushed far to the inverted

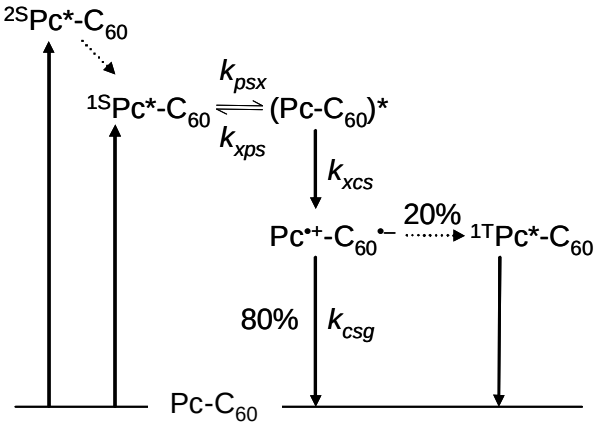

Figure 4.12. Reaction scheme for photoinduced electron transfer in **H_2Pc-C_{60}tb** and **ZnPc-C_{60}tb** in toluene.

region in non-polar toluene (see discussion and Figure 2.3 in section 2.1.2), the triplet formation becomes a significant competing reaction path.

The actual transition from the CS state to the phthalocyanine triplet can not be time-resolved with the flash-photolysis instrument nor with pump-probe, as the process falls just in the time gap of these two instruments, and this transition is given as a dotted arrow in Figure 4.12, but existence of the triplet state can be clearly indentified from the transient absorption spectra. The final spectrum of the pump-probe measurements (representing the CS state) is clearly different in shape compared to the spectrum detected with flash-photolysis: the higher absorbance around 500 nm and lower absorbance above 800 nm identify the state as the triplet state of phthalocyanine (Figure 4.13).

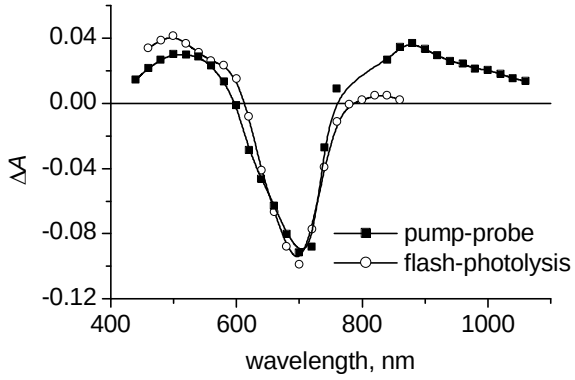

Figure 4.13. Comparison of the final decay component spectrum resolved in the pump-probe measurements to the first (and last) decay component spectrum resolved in flash-photolysis for **H_2Pc-C_{60}tb** in toluene. The spectrum from the flash-photolysis measurements has been multiplied by 6 for comparison.

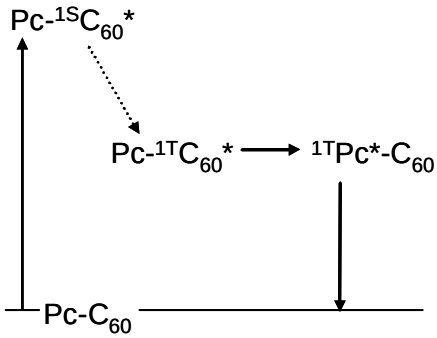

Figure 4.14. Reaction scheme for photoinduced triplet-triplet energy transfer reaction in **H_2Pc-C_{60}tb** and **ZnPc-C_{60}tb** in benzonitrile.

Actually formation of the phthalocyanine triplet state was observed in the flash-photolysis measurements for **H_2Pc-C_{60}tb** and **ZnPc-C_{60}tb** in benzonitrile, too. However, to achieve this, the C_{60} chromophore of the dyads should be excited (Figure 4.14) instead of phthalocyanine as in the general scheme of Figure 4.6. Formation of the phthalocyanine triplet state occurs via triplet-triplet energy transfer from the fullerene triplet state. Such scheme is rather surprising, because based on previous studies of porphyrin-fullerene dyads [19], which otherwise behave very similar to the phthalocyanine-fullerene dyads, one would expect efficient ET also when fullerene is excited. Since the slow intersystem crossing $Pc-{}^{1S}C_{60}* \rightarrow Pc-{}^{1T}C_{60}*$ can be detected, the competing reaction of ET from $Pc-{}^{1S}C_{60}*$ must be very inefficient in the dyads **H_2Pc-C_{60}tb** and **ZnPc-C_{60}tb**.

All of the triplet state interactions discussed above are energetically feasible as was confirmed by determining the triplet state energies of the reference phthalocyanines **H_2Pctb** and **ZnPctb** by phosphorescence measurements [IV].

4.3 Comparison of phytochlorin-, porphyrin-, and phthalocyanine-fullerene dyads

As mentioned in section 2.2.1 porphyrins and phthalocyanines both are synthetic models of chlorophyll and it is interesting to compare donor-acceptor dyads based on these two donor molecules and fullerene acceptor. Another chlorophyll-like compound is phytochlorin, which has also been studied as an electron donor linked with fullerene as the acceptor. Focus of this section is on dyads with molecular structures designed to obtain a beneficial face-to-face orientation of the donor and fullerene for efficient ET. Detailed description of the study of these compounds is given in references 12,14,15,19,32,51-53,57 and 80, and in papers III and IV. For comparison,

reactions of porphyrin-fullerene dyads with edge-to-edge orientation [V,VI] will be outlined briefly.

A wide range of phytochlorin- and porphyrin-fullerene dyads with a rigid linker joining the chromophores have been studied. Depending on the structure of the linker the energetically favourable orientation of the donor and acceptor may be an extended edge-to-edge orientation [V,VI] or a folded face-to-face orientation [12,14,15,32]. More symmetric, face-to-face structures have been obtained by connecting the donor and acceptor with two linkers [19,53]. The face-to-face orientations are characterized by interactions of the donor and acceptor resulting in visible perturbations of the steady state absorption and emission spectra [12,14,15,19,32,53]. These perturbations can be attributed to CT complex or exciplex formation, which accounts for the major difference in the reaction schemes of photoinduced electron transfer in the face-to-face donor-acceptor dyads compared to the edge-to-edge dyads.

The porphyrin-fullerene dyad compounds reported in papers V and VI all exhibit rigid, edge-to-edge orientation with r_{DA} = 14-15 Å. Moderately efficient electron transfer ($k_{ET} \sim 1\times10^{10}$ s^{-1}) in polar benzonitrile occurs in these dyads after excitation of the porphyrin chromophore. However, electron transfer does not take place in non-polar solvents, but instead energy transfer from the porphyrin singlet excited state to the fullerene singlet excited state occurs. The energy transfer is followed by intersystem crossing to the fullerene triplet excited state and finally relaxation to the ground state. The efficiency of the energy transfer reaction arises from the similar singlet excited state energies of porphyrin and fullerene, *i.e.* from the overlap of the porphyrin emission and fullerene absorption spectra.

The comparable energies of the singlet excited states of the donor and acceptor in the phytochlorin-, porphyrin- and phthalocyanine-fullerene dyads results also in the tendency of exciplex formation [14], if additionally the chromophores are in close, face-to-face contact with each other. The exciplex has been found to be a preceding state for the CS state in the photoinduced ET reaction of several dyads [14,15,19,51,52,80,IV]. The scheme (Figure 4.15) with the exciplex intermediate followed by the formation of the CS state can be proposed as the general scheme for the phytochlorin-, porphyrin- and phthalocyanine-fullerene dyads with close contact of the donor and acceptor π-electron systems. The scheme has been verified by spectroscopic measurements in both polar and non-polar solvents for most of the phytochlorin- and phthalocyanine-fullerene dyads [80,IV]. For some of the dyads the exciplex could not be detected in polar solvent [14,15] and for others the CS state could not be seen in non-polar solvent [14,15,19,51]. The reason for not seeing a state in the time-resolved

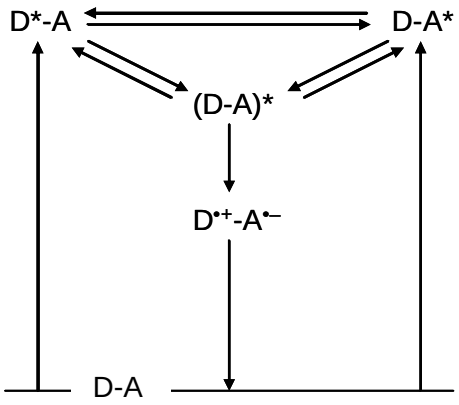

Figure 4.15. General reaction scheme for ET reactions of phytochlorin-, porphyrin- and phthalocyanine-fullerene dyads, in which the donor and acceptor moieties are in close contact. The locally excited states of the donor, D*−A, and acceptor, D−A*, are the first excited singlet states. The higher excited states and the triplet states have been omitted for clarity.

measurements can be that the state in question is formed with a much slower rate than that of its decay [14,19].

All of the transitions denoted in Figure 4.15 may not be relevant for all of the dyads discussed here. The structural differences result in differences in the energies of the different states making some of the transitions energetically more favourable and others less efficient. For instance the energy gap between the locally excited states D*−A and D−A* is smaller for the phytochlorin-fullerene dyads than for the porphyrin-fullerene dyads making the energy transfer between the two states more efficient in the former [51]. However, the energies of D*−A and D−A* are even closer to each other in the phthalocyanine-fullerene dyads, but no signs of energy transfer were detected for these dyads. Most probably this is due to the large driving force for ET resulting in the extremely fast formation of the CS state from D*−A via the exciplex [III,IV].

Table 4.4 summarizes the essential parameters of the photoinduced ET reaction for selected free-base dyads (Figure 4.16), including double-linked phthalocyanine- (**H_2Pc-C_{60}tb** [IV]) and porphyrin-fullerene (**TBD6be** [19,53]) dyads and single-linked porphyrin- (**H_2P-C1-C_{60}** [14]) and phytochlorin-fullerene (**n-PaF** [80]) dyads. The centre-to-centre distance, r_{DA}, is similar for the single-linked dyads **H_2P-C1-C_{60}** and **n-PaF**, somewhat longer for the double-linked phthalocyanine-fullerene dyad **H_2Pc-C_{60}tb** and shorter for the double-linked porphyrin-fullerene dyad **TBD6be**. It should be noted that the r_{DA} estimation of **H_2Pc-C_{60}tb** is for the so-called extended conformer, which was found to dominate over the folded conformer with r_{DA} = 6.5 Å [III].

Table 4.4. D-A centre-to-centre distances (r_{DA}), state energies, and rate constants for ET reactions of selected phthalocyanine-, porphyrin- and phytochlorin-fullerene dyads in benzonitrile. Notations: *p* = first excited singlet state of the donor, *x* = exciplex, *cs* = CS state, *g* = ground state.

compound	r_{DA} /Å	E_p /eV	E_x /eV	E_{cs} [a] /eV	k_{px} /10^9 s^{-1}	k_{xp} /10^9 s^{-1}	k_{xcs} /10^9 s^{-1}	k_{csg} /10^9 s^{-1}
H_2Pc-C_{60}tb [IV]	13	1.70	1.67	1.20	1800	620	290	14
TBD6be [19,53]	7	1.91	1.52	1.52	8300		150	2.2
H_2P-C1-C_{60} [14]	10.9	1.91	1.92		7.6	11	7	~0.5[b]
n-PaF [80]	10	1.87	1.84	1.35	210	70	250	17

[a] Taking the Coulombic interactions into account, see eq. 9.

[b] The value is not accurate, because it falls outside the pump-probe measurement range.

Even though the distance of the donor and acceptor is almost doubled in the extended conformer of **H_2Pc-C_{60}tb** compared to **TBD6be**, the rate constants for the two dyads are of the same order of magnitude. Comparison of the two porphyrin-fullerene dyads **TBD6be** and **H_2P-C1-C_{60}** shows that the close contact of the donor and acceptor achieved in **TBD6be** results in considerable increase in the rate constants. However, the comparable rate constants of **H_2Pc-C_{60}tb** and **TBD6be** can be rationalized taking into account the differences in the state energies, *i.e.* in the free energies of the reaction steps. The oxidation potential of phthalocyanine is lower than that of porphyrin, resulting in lower CS state energy. The lower CS state energy causes an increase of $-\Delta G$ for the ET reaction and a decrease in $-\Delta G$ for the BET reaction. As discussed in section 2.1 the rate constant k_{ET} increases with increasing $-\Delta G$ for ET occurring in the normal

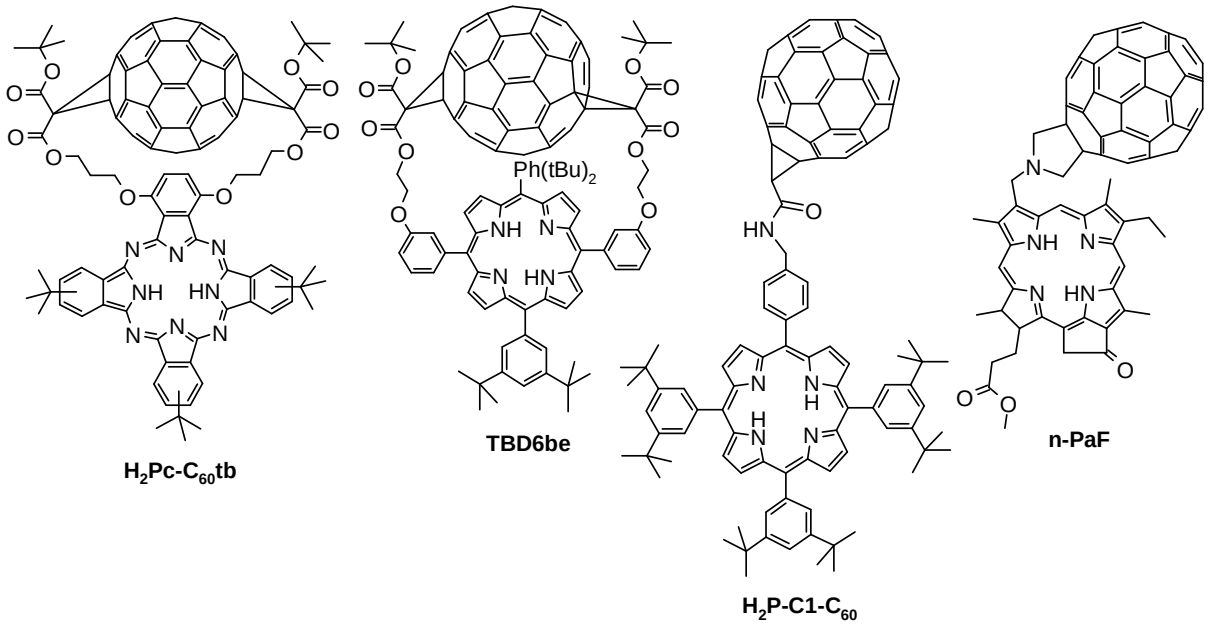

Figure 4.16. Molecular structures of dyads compared in Table 4.4.

region and rate constant k_{BET} increases with decreasing $-\Delta G$ for BET occurring in the inverted region. Thus, the favourable energetic scheme of **H_2Pc-C_{60}tb** seems to compensate the unfavourable orientation of the donor and acceptor compared to **TBD6be**, resulting in the approximately same efficiency of the reactions.

An equilibrium between D*−A and (D−A)* was observed for the phthalocyanine-fullerene dyads [III,IV], for the phytochlorin-fullerene dyads [80], and for some of the porphyrin-fullerene dyads [14]. Common structural feature of all these compounds is that the chromophores are somewhat extended further from each other (r_{DA} = 10-13 Å) than in the other dyads compared here resulting in weaker D−A electronic coupling and therefore in exciplex energy quite close to the locally excited state energies (Table 4.4) as opposed to dyads with closer D−A face-to-face contact, in which the exciplexes have energies nearer to the CS state energies [53]. In most cases the rate for the transition D*−A → (D−A)* is higher than that for the back reaction (an exception is a single linked free-base porphyrin-fullerene dyad **H_2P-C1-C_{60}**, see Table 4.4). Both of the rates increase in the following order of the dyads: porphyrin-fullerene < phytochlorin-fullerene < phthalocyanine-fullerene. Also the following formation of the CS state (D−A)* → $D^{\bullet+}-A^{\bullet-}$ is an order of magnitude faster for the phytochlorin- and phthalocyanine-fullerene dyads than for porphyrin-fullerene dyads.

The factors effecting the lifetime of the CS state are the CS distance and $-\Delta G$ for the BET reaction, *i.e.* r_{DA} and E_{cs}, respectively (Table 4.4). Comparing the r_{DA} values and BET rate constants, k_{csg}, of the different dyads in Table 4.4, it is clear that the longest CS distance does not directly result in the longest CS state lifetime. The phthalocyanine-fullerene dyad **H_2Pc-C_{60}tb** has clearly the longest r_{DA}, but BET occurs considerably faster in this dyad compared to the porphyrin-fullerene dyads **TBD6be** and **H_2P-C1-C_{60}** with shorter r_{DA}. Unfortunately E_{cs} was not available for the dyad with the longest CS state lifetime, **H_2P-C1-C_{60}**. Assuming that the redox potentials of porphyrin and fullerene are similar to those of **TBD6be**, which is quite reasonable considering the similar substituents of the porphyrin moieties, the CS state energy of **H_2P-C1-C_{60}** can be estimated to be 1.55 eV (taking into account the longer D-A distance, *i.e.* weaker Coulombic interactions). Thus, dyad **H_2P-C1-C_{60}** has the largest $-\Delta G$ for BET and slowest k_{csg} consistent with the conclusion that BET occurs in the inverted region for the discussed dyads.

5 Conclusions

The following conclusions can be drawn based on the reported results:

1. Photoinduced electron transfer of the various phthalocyanine-fullerene dyad and porphyrin-porphyrin-fullerene triad compounds studied was found to be very efficient even in a non-polar solvent, such as toluene. The rapid electron transfer reactions observed in all the compounds are consistent with the symmetric, double-linker design strategy of the molecular structures.
2. Attaching a side porphyrin unit to the previously studied porphyrin-fullerene dyad to form a triad molecule resulted in the expected prolongation of the lifetime of the charge-separated state.
3. The inner porphyrin and fullerene of the studied triads were found to act as a unit behaving in the same manner as in the corresponding dyad molecules, *e.g.* forming an exciplex with distinct emission in non-polar solvent.
4. Consistently with the studies of the triads in solutions, the photovoltaic behaviour of solid monolayer film samples of Zn porphyrin-free-base porphyrin-fullerene triads is improved considerably compared to the corresponding dyad films due to the higher absorbance and the longer charge separation distance.
5. The phthalocyanine-fullerene dyads follow the same general reaction scheme of photoinduced electron transfer as the previously studied porphyrin- and phytochlorin-fullerene dyads. The scheme includes an intermediate exciplex state preceding the charge-separated state.
6. Because of the rapid electron transfer forming the charge-separated state in the phthalocyanine-fullerene dyads, the characteristic exciplex emission is quenched efficiently and observed only weakly in the steady state emission spectra.

References

1. *Basic Research Needs for Solar Energy Utilization, Report on the Basic Energy Sciences Workshop on Solar Energy Utilization*, The U.S. Department of Energy (DOE) Office of Basic Energy Sciences, April 18–21, 2005, http://www.sc.doe.gov/bes/reports/files/SEU_rpt.pdf.
2. K. L. Chopra, P. D. Paulson and V. Dutta, *Prog. Photovolt: Res. Appl.* **2004**, *12*, 69-92.
3. D. Gust and T. A. Moore, *Science* **1989**, *244*, 35-41.
4. D. Gust, T. A. Moore and A. L. Moore, *Acc. Chem. Res.* **2001,** *34*, 40-48.
5. M. R. Wasielewski, *Chem. Rev.* **1992**, *92*, 435-461.
6. T. J. Meyer, *Acc. Chem. Res.* **1989**, *22*, 163-170.
7. D. Gust, T. A. Moore and A. L. Moore, *Acc. Chem. Res.* **1993,** *26***,** 198-205.
8. H. Imahori, Y. Mori and Y. Matano, *J. Photochem. Photobiol. C* **2003**, *4*, 51-83.
9. D. Kuciauskas, S. Lin, G. R. Seely, A. L. Moore, T. A. Moore, D. Gust, T. Drovetskaya, C. A. Reed and P. D. W. Boyd, *J. Phys. Chem.* **1996**, *100*, 15926-15932.
10. E. Dietel, A. Hirsch, J. Zhou and A. Rieker, *J. Chem. Soc., Perkin Trans. 2* **1998**, *6*, 1357-1364.
11. D. I. Schuster, *Carbon* **2000**, *3*, 1607-1614.
12. H. Imahori, N. V. Tkachenko, V. Vehmanen, K. Tamaki, H. Lemmetyinen, Y. Sakata and S. Fukuzumi, *J. Phys. Chem. A* **2001**, *105*, 1750-1756.
13. F. D'Souza, S. Gadde, M. E. Zandler, K. Arkady, M. E. El-Khouly, M. Fujitsuka and O. Ito, *J. Phys. Chem. A* **2002**, *106*, 12393-12404.
14. T. J. Kesti, N. V. Tkachenko, V. Vehmanen, H. Yamada, H. Imahori, S. Fukuzumi and H. Lemmetyinen, *J. Am. Chem. Soc.* **2002**, *124*, 8067-8077.
15. N. V. Tkachenko, H. Lemmetyinen, J. Sonoda, K. Ohkubo, T. Sato, H. Imahori and S. Fukuzumi, *J. Phys. Chem. A.* **2003**, *107*, 8834-8844.
16. F. D'Souza, G. R. Deviprasad, M. E. Zandler, M. E. El-Khouly, M. Fujitsuka and O. Ito, *J. Phys. Chem. B.* **2002**, *106*, 4952-4962.
17. W. Frey, R. Klann, F. Laermer, T. Elsaesser, E. Baumann, M. Futscher and H. A. Staab, *Chem. Phys. Lett.* **1992**, *190*, 567-573.

18. T. Häberle, J. Hirsch, F. Pöllinger, H. Heitele, M. E. Michel-Beyerle, C. Anders, A. Döhling, C. Krieger, A. Ruckemann and H. A. Staab, *J. Phys. Chem.* **1996**, *100*, 18269-18274.
19. V. Chukharev, N. V. Tkachenko, A. Efimov, D. M. Guldi, A. Hirsch, M. Scheloske and H. Lemmetyinen, *J. Phys. Chem. B* **2004**, *108*, 16377-16385.
20. T. G. Linssen, K. Dürr, M. Hanack and A. Hirsch, *J. Chem. Soc., Chem. Commun.* **1995**, 103-104.
21. Á. Sastre, A. Gouloumis, P. Vázquez, T. Torres, V. Doan, B. J. Schwartz, F. Wudl, L. Echegoyen and J. Rivera, *Org. Lett.* **1999**, *1*, 1807-1810
22. P. Zhu, P. Wang, W. Qiu, Y. Liu, C. Ye, G. Fang and Y. Song, *Appl. Phys. Lett.* **2001**, *78*, 1319-1321.
23. D. M. Guldi, J. Ramey, M. V. Martinez-Diaz, A. de la Escosura, T. Torres, T. Da Ros and M. Prato, *Chem. Commun.* **2002**, *67***,** 2774-2775.
24. F. D'Souza and O. Ito, *Coord. Chem. Rev.* **2005**, *249*, 1410-1422.
25. B. Ballesteros, G. de la Torre, T. Torres, G. L. Hug, G. M. A. Rahman and D. M. Guldi, *Tetrahedron* **2006**, *62*, 2097-2101.
26. A. de la Escosura, M. V. Martinez-Diaz, D. M. Guldi and T. Torres, *J. Am. Chem. Soc.* **2006**, *128*, 4112-4118.
27. S.-G. Liu, Y.-Q. Liu, Y. Xu, X.-Z. Jiang and D.-B. Zhu, *Tetrahedron Lett.* **1998**, *39*, 4271-4274.
28. S. Fukuzumi, K. Ohkubo, J. Ortiz, A. M. Gutiérrez, F. Fernández-Lázaro and Á. Sastre-Santos, *Chem. Commun.* **2005**, 3814-3816.
29. M. R. Wasielewski, D. W. Minsek, M. P. Niemczyk, W. A. Svec and N. C. Yang, *J. Am. Chem. Soc.* **1990**, *112*, 2823-2824.
30. N. Mataga, A. Karen, T. Okada, S. Nishitani, N. Kurata, Y. Sakata and S. Misumi, *J. Phys. Chem.* **1984**, *88*, 5138-5141.
31. D. M. Guldi, M. Maggini, G. Scorrano and M. Prato, *J. Am. Chem. Soc.* **1997**, *119*, 974-980.
32. V. Vehmanen, N. V. Tkachenko, H. Imahori, S. Fukuzumi and H. Lemmetyinen, *Spectrochim. Acta, Part A* **2001**, *57*, 2229-2244.
33. K. Kamioka, R. A. Cormier, T. W. Lutton and J. S. Connolly, *J. Am. Chem. Soc.* **1992,** *114*, 4414-4415.
34. N. Martín, L. Sánchez, B. Illescas and I. Pérez, *Chem. Rev.* **1998,** *98*, 2527-2547.

35. T. A. Moore, D. Gust, P. Mathis, J.-C. Mialocq, C. Chachaty, R. V. Bensasson, E. J. Land, D. Doizi, P. A. Liddell, W. R. Lehman, G. A. Nemeth and A. L. Moore, *Nature* **1984**, *307*, 630-632.
36. D. Gust, T. A. Moore, A. L. Moore, A. N. Macpherson, A. Lopez, J. M. DeGraziano, I. Gouni, E. Bittersmann, G. R. Seely, F. Gao, R. A. Nieman, X. C. Ma, L. J. Demanche, S.-C. Hung, D. K. Luttrull, S.-J. Lee and P. K. Kerrigan, *J. Am. Chem. Soc.* **1993**, *115*, 11141-11152.
37. P. A. Liddell, D. Kuciauskas, J. P. Sumida, B. Nah, D. Nguyen, A. L. Moore, T. A. Moore and D. Gust, *J. Am. Chem. Soc.* **1997**, *119*, 1400-1405.
38. D. Kuciauskas, P. A. Liddell, S. Lin, T. E. Johnson, S. J. Weghorn, J. S. Lindsey, A. L. Moore, T. A. Moore and D. Gust, *J. Am. Chem. Soc.* **1999**, *121*, 8604-8614.
39. C. Luo, D. M. Guldi, H. Imahori, K. Tamaki and Y. Sakata, *J. Am. Chem. Soc.* **2000**, *122*, 6535-6551.
40. G. Kodis, P. A. Liddell, L. de la Garza, P. C. Clausen, J. S. Lindsey, A. L. Moore, T. A. Moore and D. Gust, *J. Phys. Chem. A* **2002**, *106*, 2036-2048.
41. P. A. Liddell, G. Kodis, L. de la Garza, A. L. Moore, T. A. Moore and D. Gust, *J. Phys. Chem. B* **2004**, *108*, 10256-10265.
42. F. D'Souza, P. M. Smith, S. Gadde, A. L. McCarty, M. J. Kullman, M. E. Zandler, M. Itou, Y. Araki and O. Ito, *J. Phys. Chem. B* **2004**, *108*, 11333-11343.
43. G. L. Closs and J. R. Miller, *Science* **1988**, *240*, 440-447.
44. J.-P. Bourgeois, F. Diederich, L. Echegoyen and J.-F. Nierengarten, *Helv. Chim. Acta* **1998**, *81*, 1835-1844.
45. E. Dietel, A. Hirsch, E. Eichhorn, A. Rieker, S. Hackbarth and B. Roder, *Chem. Commun.* **1998**, 1981-1982.
46. D. I. Schuster, P. Cheng, S. R. Wilson, V. Prokhorenko, M. Katterle, A. R. Holzwarth, S. E. Braslavsky, G. Klihm, R. M. Williams and C. Luo, *J. Am. Chem. Soc.* **1999**, *121*, 11599-11600.
47. A. Efimov, P. Vainiotalo, N. Tkachenko and H. Lemmetyinen, *J. Porphyrins Phthalocyanines* **2004**, *7*, 610-616.
48. V. Chukharev, T. Vuorinen, A. Efimov, N. V. Tkachenko, M. Kimura, S. Fukuzumi, H. Imahori and H. Lemmetyinen, *Langmuir* **2005**, *21*, 6385-6391.
49. T. Vuorinen, K. Kaunisto, N. V. Tkachenko, A. Efimov, A. S. Alekseev, K. Hosomizu, H. Imahori and H. Lemmetyinen, *Langmuir* **2005**, *21*, 5383-5390.

50. H. Lehtivuori, H. Lemmetyinen and N. V. Tkachenko, *J. Am. Chem. Soc.* **2006**, *128*, 16036-16037.
51. N. V. Tkachenko, L. Rantala, A. Y. Tauber, J. Helaja, P. H. Hynninen and H. Lemmetyinen, *J. Am. Chem. Soc.* **1999**, *121*, 9378-9387.
52. V. Vehmanen, N. V. Tkachenko, A. Y. Tauber, P. H. Hynninen and H. Lemmetyinen, *Chem. Phys. Lett.* **2001**, *345*, 213-218.
53. V. Chukharev, N. V. Tkachenko, A. Efimov and H. Lemmetyinen, *Chem. Phys. Lett.* **2005**, *411*, 501-505.
54. R. A. Marcus, *Rev. Mod. Phys.* **1993**, *65*, 599-610.
55. J. R. Bolton and M. D. Archer, *Adv. Chem. Ser.* **1991**, *228*, 7-23.
56. I. R. Gould, R. H. Young, L. J. Mueller and S. Farid, *J. Am. Chem. Soc.* **1994**, *116*, 8176-8187.
57. V. Vehmanen: *Photoinduced Electron Transfer in Porphyrin-Fullerene and Phytochlorin-Fullerene Dyads*, Doctoral Thesis, Tampere University of Technology Publications 387, Tampere, **2002**.
58. S. L. Mattes and S. Farid, *Science* **1984**, *226*, 917-921.
59. V. Chukharev, N. Tkachenko, A. Efimov, P. Vainiotalo and H. Lemmetyinen, *Photochem. Photobiol. Sci.* **2003**, *2*, 1044-1049.
60. P. H. Kwan and T. M. Swager, *J. Am. Chem. Soc.* **2005**, *127*, 5902-5909.
61. B. Pispisa, M. Venanzi, A. Palleschi and G. Zanotti, *J. Photochem. Photobiol., A* **1997**, *105*, 225-233.
62. P.-C. Lo, X. Leng and D. K. P. Ng, *Coord. Chem. Rev.* **2007**, *251*, 2334-2353.
63. H. W. Kroto, J. R. Heath, S. C. O'Brien, R. F. Curl and R.E. Smalley, *Nature* **1985**, *318*, 162-163.
64. W. Krätschmer, L. D. Lamb, K. Fostiropoulos and D. R. Huffman, *Nature* **1990**, *347*, 354-358.
65. S. Larsson, A. Klimkāns, L. Rodriguez-Monge and G. Duškesas, *THEOCHEM* **1998**, *425*, 155-159.
66. D. M. Guldi and M. Prato, *Acc. Chem. Res.* **2000**, *33*, 695-703.
67. H. Imahori, K. Hagiwara, T. Akiyama, M. Aoki, S. Taniguchi, T. Okada, M. Shirakawa and Y. Sakata, *Chem. Phys. Lett.* **1996**, *263*, 545-550.
68. D. M. Guldi, I. Zilbermann, A. Gouloumis, P. Vázquez and T. Torres, *J. Phys. Chem. B* **2004**, *108*, 18485-18494.
69. L. Echegoyen and L. E. Echegoyen, *Acc. Chem. Res.* **1998**, *31*, 593-601.

70. E. H. Yonemoto, G. B. Saupe, R. H. Schmehl, S. M. Hubig, R. L. Riley, B. L. Iverson and T. E. Mallouk, *J. Am. Chem. Soc.* **1994**, *116*, 4786-4795.
71. J. Wiberg, L. Guo, K. Pettersson, D. Nilsson, T. Ljungdahl, J. Mårtensson and B. Albinsson, *J. Am. Chem. Soc.* **2007**, *129*, 155-163.
72. D. M. Guldi, C. Luo, M. Prato, A. Troisi, F. Zerbetto, M. Scheloske, E. Dietel, W. Bauer and A. Hirsch, *J. Am. Chem. Soc.* **2001**, *123*, 9166-9167.
73. N. V. Tkachenko: *Optical Spectroscopy Methods and Instrumentations*, Elsevier, Amsterdam **2006**.
74. G. J. Kavarnos: *Fundamentals of Photoinduced Electron Transfer*, VCH Publishers, Inc., New York **1993**.
75. N. V. Tkachenko, A. Y. Tauber, P. H. Hynninen, A. Y. Sharonov and H. Lemmetyinen, *J. Phys. Chem. A* 1999, **103**, 3657-3665.
76. T. Vuorinen, K. Kaunisto, N. V. Tkachenko, A. Efimov, H. Lemmetyinen, A. S. Alekseev, K. Hosomizu and H. Imahori, *Langmuir* **2005**, *21*, 5383-5390.
77. N. V. Tkachenko, E. Vuorimaa, T. Kesti, A. S. Alekseev, A. Y. Tauber, P. H. Hynninen and H. Lemmetyinen, *J. Phys. Chem. B* **2000**, *104*, 6371-6379.
78. H. Chou, C.-T. Chen, K. F. Stork, P. W. Bohn and K. S. Suslick, *J. Phys. Chem.* **1994**, *98*, 383-385.
79. J. Zak, H. Yuan, M. Ho, L. K. Woo and M. D. Porter, *Langmuir* **1993**, *9*, 2772-2774.
80. V. Vehmanen, N. V. Tkachenko, A. Efimov, P. Damlin, A. Ivaska and H. Lemmetyinen, *J. Phys. Chem. A* **2002**, *106*, 8029-8038.
81. T. Nojiri, M. M. Alam, H. Konami, A. Watanabe and O. Ito, *J. Phys. Chem. A* **1997**, *101*, 7943-7947.
82. M. Asano-Someda and Y. Kaizu, *J. Photochem. Photobiol., A* **1995**, *87*, 23-29.